Bulk Parameterization of Air–Sea Fluxes: Updates and Verification for the COARE Algorithm

C. W. FAIRALL

NOAA/Environmental Technology Laboratory, Boulder, Colorado

E. F. BRADLEY

CSIRO Land and Water, Canberra, Australia

J. E. HARE AND A. A. GRACHEV

Cooperative Institute for Research in Environmental Sciences, University of Colorado, and NOAA/Environmental Technology Laboratory, Boulder, Colorado

J. B. EDSON

Woods Hole Oceanographic Institution, Woods Hole, Massachusetts

(Manuscript received 8 November 2001, in final form 15 May 2002)

ABSTRACT

In 1996, version 2.5 of the Coupled Ocean–Atmosphere Response Experiment (COARE) bulk algorithm was published, and it has become one of the most frequently used algorithms in the air–sea interaction community. This paper describes steps taken to improve the algorithm in several ways. The number of iterations to solve for stability has been shortened from 20 to 3, and adjustments have been made to the basic profile stability functions. The scalar transfer coefficients have been redefined in terms of the mixing ratio, which is the fundamentally conserved quantity, rather than the measured water vapor mass concentration. Both the velocity and scalar roughness lengths have been changed. For the velocity roughness, the original fixed value of the Charnock parameter has been replaced by one that increases with wind speeds of between 10 and 18 m s^{-1}. The scalar roughness length parameterization has been simplified to fit both an early set of NOAA/Environmental Technology Laboratory (ETL) experiments and the Humidity Exchange Over the Sea (HEXOS) program. These changes slightly increase the fluxes for wind speeds exceeding 10 m s^{-1}. For interested users, two simple parameterizations of the surface gravity wave influence on fluxes have been added (but not evaluated).

This new version of the algorithm (COARE 3.0) was based on published results and 2777 1-h covariance flux measurements in the ETL inventory. To test it, 4439 new values from field experiments between 1997 and 1999 were added, which now dominate the database, especially in the wind speed regime beyond 10 m s^{-1}, where the number of observations increased from 67 to about 800. After applying various quality controls, the database was used to evaluate the algorithm in several ways. For an overall mean, the algorithm agrees with the data to within a few percent for stress and latent heat flux. The agreement is also excellent when the bulk and directly measured fluxes are averaged in bins of 10-m neutral wind speed. For a more stringent test, the average 10-m neutral transfer coefficients were computed for stress and moisture in wind speed bins, using different averaging schemes with fairly similar results. The average (mean and median) model results agreed with the measurements to within about 5% for moisture from 0 to 20 m s^{-1}. For stress, the covariance measurements were about 10% higher than the model at wind speeds over 15 m s^{-1}, while inertial-dissipation measurements agreed closely at all wind speeds. The values for stress are between 8% (for inertial dissipation) and 18% (for covariance) higher at 20 m s^{-1} than two other classic results. Twenty years ago, bulk flux schemes were considered to be uncertain by about 30%; the authors find COARE 3.0 to be accurate within 5% for wind speeds of 0–10 m s^{-1} and 10% for wind speeds of between 10 and 20 m s^{-1}.

1. Introduction

The Coupled Ocean–Atmosphere Response Experiment (COARE; Webster and Lukas 1992) triggered a resurgence of interest in measurement and parameterization of air–sea turbulent and radiative fluxes. The program set a 10 W m^{-2} goal for the total uncertainty in long-term (~1 month) measurement of the surface energy budget for the COARE region. A COARE Flux Working Group (FWG) was formed, which developed a plan for pre-COARE flux cruises, intercomparisons between ships, buoys, and aircraft during COARE, and post-COARE field efforts and calibration studies (Bradley and Weller 1997). Flux estimates originated from

Corresponding author address: Dr. C. W. Fairall, NOAA/Environmental Technology Lab., David Skaggs Research Center, 325 Broadway, Boulder, CO 80305.
E-mail: chris.fairall@noaa.gov

ship, buoy, aircraft, satellite, and model data, so to ensure compatibility when comparing results the FWG developed a bulk turbulent flux algorithm as a common standard. The new algorithm needed to accommodate the light wind conditions and large near-surface ocean temperature gradients often encountered in this region. It evolved over several years and was eventually frozen at version 2.5b and published (Fairall et al. 1996a).

The algorithm was developed using COARE measurements, albeit with a relatively limited wind speed range (0–12 m s^{-1}), and has been used by many research groups for COARE analyses (more than 200 citations at the time of this writing). However, it has also been used outside the Tropics in a wide variety of conditions, raising obvious questions about its applicability in colder waters, midlatitudes, and much higher wind speeds. The algorithm was ''globalized'' in the sense that, wherever possible, physical variables are computed as functions of ambient conditions (e.g., temperature, latitude, solar flux) rather than hardwired to tropical values. Since 1996, work has continued to extend it to higher wind speeds and to verify it against high-quality data outside the Tropics. In 1998 a new version was developed (Bradley et al. 2000), based on six National Oceanic and Atmospheric Administration (NOAA) Environmental Technology Laboratory (ETL) cruises conducted between 1991 and 1993, preliminary results from two other ETL programs, and other published measurements from high wind regions, to extend the applicability to 20 m s^{-1}. It has evolved continuously since then, and is now considered ready for public release as COARE 3.0. Between 1997 and 1999 ETL conducted six more cruises, obtaining direct covariance and inertial-dissipation flux estimates and high-quality bulk meteorological variables, suitable for verifying the new algorithm.

In this paper we describe the new version of the COARE algorithm and its verification. Following this introduction, we give some general background on flux algorithms and the original COARE version (section 2). The new version of the algorithm is described in detail in section 3, and evaluated against the entire ETL database of 7216 1-h values obtained between 1991 and 1999. In section 5 we discuss these results in relation to other algorithms and other measurements. Our conclusions are given in section 6. The measurement system, flux processing methods, and accuracy issues are discussed in the appendix.

2. Background on similarity relationships and flux algorithms

a. Bulk scaling theory

The conservation equation for the ensemble mean of variable x, denoted as X, is

$$\frac{\partial X}{\partial t} + \nabla_h X \cdot \mathbf{U}_h = -\frac{\partial(\overline{w'x'})}{\partial z} + \overline{I_x}, \qquad (1)$$

where the subscript h denotes horizontal components and I_x represents the source term. The quantity of interest is the Reynolds flux enclosed in parentheses. It can be determined by measuring the time or space series of w' and x' and computing their mean product; this is referred to as the covariance or eddy-correlation method, and is the only direct flux measurement. There are also many indirect approaches to flux estimation. The inertial-dissipation (ID) method uses characteristics of the inertial subrange of atmospheric velocity and scalar turbulence spectra (Fairall and Larsen 1986; Edson et al. 1991). Details are given in the appendix. Other schemes are based on applications of the Monin–Obukhov similarity theory (MOST) to measured atmospheric properties (these methods yield estimates of the surface flux only, while the covariance method is general). This diversity of flux methods is primarily due to the historical difficulty, expense, and impracticality of making covariance measurements for all variables on the horizontal and temporal scales of interest. Measurements over the ocean involve the additional complication of platform motion, flow distortion over the platform and equipment, and contamination by sea spray and salt particles. More complete information on flux methods can be found in Smith et al. (1996) or Fairall et al. (1997).

''Bulk'' algorithms to estimate surface fluxes are widely used in numerical models and in applications (e.g., satellite retrievals) where highly detailed local information is not available. These are based upon MOST representations of the fluxes in terms of mean quantities

$$\overline{w'x'} = c_x^{1/2} c_d^{1/2} S\Delta X = C_x S\Delta X, \qquad (2)$$

where x can be u, v wind components, the potential temperature, θ, the water vapor specific humidity, q (see section 3b), or some atmospheric trace species mixing ratio. Here c_x is the bulk transfer coefficient for the variable x (d being used for wind speed) and C_x is the total transfer coefficient. Here ΔX is the air–sea difference in the mean value of x, and S is the mean wind speed (relative to the ocean surface), which is composed of a mean vector part (U and V components) and a gustiness part (U_g) to account for subgrid-scale variability:

$$\Delta X = X_{\text{sea}} - X(z); \qquad S = (U^2 + V^2 + U_g^2)^{1/2}. \qquad (3)$$

The transfer coefficients have a dependence on surface stability prescribed by MOST

$$c_x^{1/2}(\zeta) = \frac{c_{xn}^{1/2}}{\left[1 - \dfrac{c_{xn}^{1/2}}{\kappa}\psi_x(\zeta)\right]};$$

$$c_{xn}^{1/2} = \frac{\kappa}{\ln(z/z_{ox})}, \qquad (4)$$

where the subscript n refers to neutral ($\zeta = 0$) stability, z is the height of measurement of the mean quantity

$X(z)$, ψ_x is an empirical function describing the stability dependence of the mean profile, κ is von Karman's constant, and z_{ox} a parameter called the roughness length that characterizes the neutral transfer properties of the surface for the quantity, x. The MOST stability parameter, ζ, is given by

$$\zeta = -\frac{\kappa g z}{T}\frac{(\overline{w'\theta'} + 0.61T\overline{w'q'})}{(-\overline{w'u'})^{3/2}}, \quad (5)$$

where T is temperature, g the acceleration due to gravity, and we are using $\overline{w'u'}$ to denote the streamwise component (see the discussion in the appendix). For later use, we define the MOST scaling parameters $u_* = \sqrt{-\overline{w'u'}}$ (also known as the friction velocity), $\theta_* = -\overline{w'\theta'}/u_*$, and $q_* = -\overline{w'q'}/u_*$ for velocity, temperature and humidity, respectively. It is sometimes convenient (e.g., to reduce variability in MOST relationships) to use a bulk stability parameter, replacing the kinematic fluxes in (5) with u_*, θ_*, q_*, obtained by iteration within the bulk algorithm.

b. COARE 2.5

The essence of a bulk model is contained in (2), (3), and (5) plus the representations (parameterizations) of the roughness lengths (or, equivalently the transfer coefficients) and the profile stability functions (ψ_x). While there are many algorithms available today, we will restrict the discussion in this section to the Tropical Ocean Global Atmosphere (TOGA) COARE bulk algorithm (Fairall et al. 1996a). Parameterizations in the original COARE model were based on those of the Liu–Katsaros–Businger model (LKB; Liu et al. 1979) but updated. The LKB model allowed for different velocity and scalar von Karman constants, giving them values of 0.35 and 0.45. For the COARE model, the velocity von Karman was set to 0.40. The velocity roughness length was specified as Charnock's (1955) expression plus a smooth flow limit, following Smith (1988):

$$z_o = \frac{\alpha u_*^2}{g} + \frac{0.11\nu}{u_*}, \quad (6)$$

where ν is the kinematic viscosity. The COARE flux data supported Smith's value of the Charnock parameter, $\alpha = 0.011$. LKB derive the scalar roughness lengths from the principles of surface renewal theory in which, across a thin ($\sim$1 mm) interfacial layer, small eddies transfer heat randomly and intermittently between the bulk fluid and the surface (Liu and Businger 1975). In COARE 2.5 we adopt the LKB representation of the scalar roughness lengths, parameterized in terms of the roughness Reynolds number ($R_r = z_o u_*/\nu$):

$$z_{ox} = \frac{\nu}{u_*} f_x(R_r), \quad (7)$$

where scalar roughness Reynolds numbers are $R_x = u_* z_{ox}/\nu$ (see section 3e and Fig. 13). The LKB specification of scalar roughness (7) was retained and the scalar von Karman constant was adjusted to reproduce the average observed latent heat flux over the entire field program; this resulted in a value of 0.40 (i.e., the same as for velocity).

The profile stability functions are a blend of the familiar Kansas expressions (Businger et al. 1971) near neutral with a form that obeys the theoretical scaling limit in highly convective conditions (Fairall et al. 1996a). The addition of gustiness solved the mathematical problem of producing finite scalar fluxes as the wind speed approached zero. In the COARE algorithm, the gustiness is represented as boundary layer–scale eddies using the convective velocity scale, W_*,

$$U_g = \beta W_* = \beta\left(\frac{g}{T}\overline{w'\theta_v'}z_i\right)^{1/3}, \quad (8)$$

where z_i is the depth of the convective boundary layer, θ_v is the virtual potential temperature, and β is a parameter presently set to 1.25. If gustiness is not used, then the behavior of the ψ_x functions as $|\zeta| \to \infty$ becomes critical in determining fluxes in light winds (Godfrey and Beljaars 1991).

In typical execution of a bulk algorithm, the atmospheric variables (U, V, T, q) at reference height z are provided through measurement or model output; the surface properties (current vector, water temperature) are also provided. Strictly speaking, (3) requires the true interface temperature, T_s, but usually only the temperature at some depth, $T_w(D)$, is available so that a method of estimating T_s from T_w is needed. The COARE algorithm incorporates submodels that represent the millimeter-scale cool skin near the interface and the diurnal (solar) warm layer in the upper few meters of the ocean (Fairall et al. 1996b; Webster et al. 1996). The cool skin implies that the true interface temperature is several tenths (°C) cooler than the bulk water near the surface. In light wind and sunny conditions the sun may warm the upper few meters of the ocean by 1°–3°C. The surface value for specific humidity is computed from the surface temperature and the vapor pressure of seawater (0.98 times the vapor pressure of pure water; Kraus and Businger 1994).

c. Discussion of recent bulk models

Almost two decades have passed since Blanc (1985) published his careful and rather alarming review of the large differences between more than 10 bulk flux algorithms. At that time, many of the physical processes involved in air–sea transfer of heat or momentum were embedded within the transfer coefficient for a particular entity. While transfer coefficients were known to be a function of wind speed, height, and atmospheric stability, more often than not the accuracy of available test data did not justify anything other than a constant value for the transfer coefficient of scalars, or a simple wind

TABLE 1. Comparative features of various modern bulk flux algorithms.

Authors	Gustiness	Stability	z_o	z_{oq}	2% vapor pressure reduction	Cool skin
ZZD	$\beta = 1.0$	Kansas (Businger et al. 1971): unstable Holtslag (1990): stable Kader and Yaglom (1990)	Smith (1988) $\alpha = 0.013$	Brutsaert (1982) $\alpha = 2.67$; $\beta = -2.57$	Yes	No
BVW	$\beta = 1.25$	Benoit (1977): unstable Benoit (1977) and Holtslag (1990): stable	Smith (1988) plus waves	$R_t = 0.40$ $R_Q = 0.62$		No
CFC	No	Benoit (1977): unstable Benoit (1977) and Holtslag (1990): stable	Same as BVW		Yes	Yes
ZM95	No	Kansas (Businger et al. 1971)	Smith (1988) $\alpha = 0.011$	2×10^{-5}		No
Beljaars (1995)	$\beta = 1.20$	Kansas (Businger et al. 1971)	Smith (1988) $\alpha = 0.018$	$R_t = 0.40$ $R_Q = 0.62$		No

speed–dependent value for stress. Such simple expressions have become inadequate for several reasons, mostly connected with the burgeoning requirements of climate research, and recognition of the sensitivity of numerical climate models to small changes in air–sea flux values, particularly when attempting to couple oceanic and atmospheric GCMs. We will briefly describe some other bulk flux algorithms that have emerged over the period of development of the COARE algorithm, and give their main features in Table 1. The list is not exhaustive or even possibly up to date.

The algorithm described by Zeng et al. (1998, hereafter ZZD) was developed to suit the needs of numerical model codes. As with COARE 2.5, ZZD use the Kansas profile functions for near-neutral atmospheric stability, with the convective forms of Kader and Yaglom (1990) and the relations of Holtslag et al. (1990) in very stable conditions. Equation (6), with $\alpha = 0.013$, is used for z_o and the Brutsaert (1982) formulation [see Eq. (29)] is used for the scalar roughness lengths, with constant coefficients obtained from the R/V *Moana Wave* COARE data (Fairall et al. 1996a). ZZD include a ''gustiness'' correction, with $\beta = 1.0$, and allowance for the 2% reduction in saturated specific humidity over seawater, which they find decreases latent heat flux by 20% at 14 m s^{-1}. The algorithm is tuned to the same dataset (the R/V *Moana Wave* observations by Fairall et al. 1996a) as COARE version 2.5 for low to moderate wind speeds, and the Humidity Exchange Over the Sea (HEXOS) data (De Cosmo et al. 1996) up to 18 m s^{-1}. However, they use the HEXOS data as presented by the authors, rather than modified as described in section 3e. Various empirical constants are given values that ensure reasonable agreement with observations over the wind speed range 0–18 m s^{-1}.

The Bourassa et al. (1999, hereafter BVW) bulk model is notable for its attempt to relate surface roughness lengths, and hence the exchange coefficients, to various aspects of sea state, swell, gravity waves, and capillary waves. They draw on, and extend, published representations of wave structure in their analyses, but adequate validating data are not yet available to test the potential of this algorithm. BVW point out that, particularly under low wind conditions where swell, wind velocity, stress, and current directions are not necessarily parallel, their algorithm allows the cross-wind component of stress to be calculated. They note that, with the coexistence of these different wave types and interactions between them, it is unclear what the proper coordinate frame of reference should be for the wind and water velocities. For z_o, BVW use a version of Eq. (6) in which the ''Charnock'' term is replaced by one involving wave parameters. For the scalar roughness lengths, they use the Reynolds parameters, $R_t = 0.4$ and $R_q = 0.62$, given by Brutsaert (1982; section 5). BVW adopt the profile stability functions of Beljaars and Holtslag (1991) for stable and of Benoit (1977) for unstable conditions, and gustiness with $\beta = 1.25$.

The Clayson et al. (1996, hereafter CFC) algorithm is based on the surface renewal theory of Brutsaert (1975), with an alternative timescale parameterization. CFC use a simplified form of the BVW sea state surface roughness model, and the same profile stability functions as BVW, which lead to Brutsaert-like expressions for the scalar roughness lengths. Unlike BVW, they do not include a gustiness term, relying on their capillary wave parameterization and surface renewal theory to obtain correct fluxes in low wind, convective conditions. Because this algorithm was developed for the assessment of fluxes from satellite data, they incorporate a model of the ocean cool skin (Wick et al. 1996). They also adjust surface humidity for the 2% reduction of vapor pressure over saline water. However, they do not correct SST for the diurnal thermocline.

Zhang and McPhaden (1995, hereafter ZM95) studied the relationship between SST and latent heat flux in the

equatorial Pacific Ocean, using data from the TOGA Tropical Atmosphere Ocean (TAO) moored array. Their bulk flux algorithm takes the simplest possible route consistent with the need to take account of low wind and highly convective conditions, and is computationally economical. They adopt the standard Kansas stability profile functions across the entire unstable range from near-neutral to free convection, and Eq. (6) with $\alpha = 0.011$ for the momentum roughness length. However, following Geernaert (1987) they set the temperature and moisture roughness lengths equal and constant at 2×10^{-5} m.

Beljaars (1995) approaches the problem from the perspective of the numerical modeler seeking economical solutions without violating physical reality. He shows that normal MOST can be used in the surface layer without modification for free convection (i.e., no ⅓ power law), as long as a convective scaling velocity [Eq. (8)] is included in the bulk equation. He adopts the standard Kansas expressions, arguing that the behavior of the stability functions for large $(-\zeta)$ is not too critical because vertical gradients are small in the well-mixed regime, and contribute little to the air–surface velocity, temperature, or moisture difference. His analysis is general for the surface layer over land and ocean, rough and smooth surfaces, and suggests a typical value $\beta = 1.2$ for the gustiness parameter. For air–sea transfer over the ocean, Beljaars (1995) uses Eq. (6) for z_o, with $\alpha = 0.018$, and the same Brutsaert (1982) expressions for the scalar roughness lengths as BVW, applied to both smooth and rough flow. He justifies this cautiously, on the grounds that empirical evidence points to an almost constant moisture transfer coefficient over the entire low to high wind speed regime (Smith 1989). Approaching zero wind speed, his transfer coefficients for both heat and moisture follow quite well the increasing trend shown by the low wind data of Bradley et al. (1991).

Using COARE and TAO mooring data, ZZD have compared momentum and scalar fluxes from several of the algorithms described above and show that, up to around 6 m s^{-1}, their performance is very similar. Differences appear at higher wind speeds, but uncertainty about the quality of the test data in this regime makes judgement difficult. ZZD also consider the parameterizations employed in several numerical models, and conclude that these are seriously defective. It is probably fair to comment that almost any of the modern algorithms, with reasonable roughness parameterizations and stability correction, would considerably improve the performance of the models.

3. Advances for COARE 3.0

For the improved algorithm three major issues were addressed. First, the COARE model was fit to the average flux observed but was not a perfect fit to the observed wind speed dependence (e.g., the peak in the 10-m neutral transfer coefficient C_{e10n} in the LKB model at wind speeds around 6 m s^{-1} was not apparent in the data). Second, the model was published as being valid over the COARE wind range from 0 to 10 m s^{-1}, and extension to higher wind speeds was needed. Third, it needed to be generalized for more global applications, and tested against a much broader dataset. Preliminary discussion of these and other minor improvements appear in Bradley et al. (2000) and Fairall et al. (2001); they are summarized as follows:

1) The empirical constant in the convective portion of the scalar profile function has been changed for improved matching to direct profile observations (Grachev et al. 2000).
2) The Kansas stable profile functions (Businger et al. 1971) have been replaced by those from Beljaars and Holtslag (1991) which, based on new profile data taken over the Arctic ice cap (Persson et al. 2002), appear to be a better fit at extreme stability.
3) The stability iteration loop has been reduced from 20 to 3 by taking advantage of a bulk Richardson number parameterization for an improved first guess (Grachev and Fairall 1997).
4) The latent heat flux has been reformulated in terms of mixing ratio instead of water vapor density.
5) Above 10 m s^{-1} the Charnock parameter takes a simple wind speed dependence based on data from various sources (e.g., Hare et al. 1999).
6) An option has been added to allow the velocity roughness to be affected by wave parameters.
7) The LKB scalar roughness relationship $[f_x(R_r)]$ has been replaced with a much simpler one that fits both the COARE and Humidity Exchange Over the Sea Main Experiment (HEXMAX) databases.

The first two changes are adjustments to the mean profile stability functions and tend to increase the scalar fluxes slightly in light winds. The second change also removes a numerical instability in extremely stable conditions (in effect, it eliminates a critical bulk Richardson number). The third change reduces calculation time significantly, which enhances suitability for incorporation in numerical models. The fourth casts the moisture transfer in the fundamentally conservative quantity (mixing ratio) rather than the quantity (water vapor density) that is actually measured by most flux systems. Thus, it eliminates the need to add a Webb et al. (1980) correction term to the computed latent heat flux. The model now returns the mean Webb velocity, which can be used to compute Webb corrections for any trace gas or particle fluxes measured simultaneously. The changes in roughness representation lead to increases in the fluxes primarily for wind speeds above 10 m s^{-1}. The wave parameterizations have been added primarily as a response to requests from various users. We have taken two models from the recent literature (Taylor and Yelland 2001; Oost et al. 2002) that are wave age and/or wave slope based.

MATLAB and FORTRAN versions of both COARE 2.5b and 3.0 have been made publicly available online at ftp://ftp.etl.noaa.gov/et7/anonymous/cfairall/bulkalg/. Included is a description of the codes and a test dataset file. The programs are set up to read the test file and output the results; output files and graphs of results are also provided.

a. Stability function considerations

The unstable profile stability functions used in the COARE algorithm are a blend of Kansas forms (valid for $-1 < \zeta < 0$) and forms that scale as $(a_x\zeta)^{-1/3}$ in convective conditions (a_x is an empirical constant and the $-1/3$ power is the asymptotic limit of MOST; see Grachev et al. 2000). In COARE 2.5 a_u and a_s were set to 12.87; Grachev et al. (2000) showed that the values $a_u = 10.15$ and $a_s = 34.15$ gave the smoothest blend of Kansas and convective forms so these values have been adopted for COARE 3.0. The modification of the profile function on the stable side is based on more extensive observations. The original Kansas observations were limited to $0 < \zeta < 1$. The form of the stable side functions as $\zeta \gg 1$ has implications for the numerical characteristics of the stability iteration.

The bulk flux relations are a set of coupled equations [Eqs. (2)–(5)] that are solved iteratively for the fluxes and the stability. In COARE 2.5 the initial stability is set to 0 and 20 iterations are used to solve the equations; in COARE 3.0 the initial stability is set to a first guess based on a bulk Richardson number (Grachev and Fairall 1997), so only three iterations are needed. If we substitute the bulk relationships into (5), then we obtain a bulk stability parameter

$$\zeta_b = C_b R_{ib} \frac{\left[1 - \frac{c_{dn}^{1/2}}{\kappa}\psi_u(\zeta)\right]^2}{\left[1 - \frac{c_{tn}^{1/2}}{\kappa}\psi_T(\zeta)\right]}, \tag{9}$$

where $C_b = \kappa c_{tn}^{1/2}/c_{dn} \approx \kappa/c_{dn}^{1/2} \approx 10$ and the bulk Richardson number, R_{ib}, is

$$R_{ib} = -\frac{gz}{T}\frac{\Delta\theta_v}{U^2}. \tag{10}$$

The behavior of (9) in unstable versus stable conditions becomes the basis of the improved first guess of ζ for the iteration. The stable functions from the Kansas experiment (which were used in COARE 2.5b) take the form

$$\psi_u = \psi_T = -B\zeta, \tag{11}$$

where B is about 5.0. Substituting (11) into (9) and ignoring the small difference in velocity and temperature transfer coefficients in the stability terms, then

$$\zeta = C_b R_{ib}(1 - BR_{ib})^{-1}, \tag{12}$$

which becomes singular when

$$R_{ib} \geq B^{-1} \approx 0.2. \tag{13}$$

This result is consistent with the original Kansas analysis that suggested a critical gradient Richardson number on the order of 0.2. The physical interpretation is debatable, but numerically the iteration based on (9) does not converge if R_{ib} exceeds the threshold described by (13). If one views this condition as complete suppression of turbulent transport, then the fluxes should simply be set to zero. Using extensive measurements from a 100-m tower over land, Beljaars and Holtslag (1991) found finite, but highly intermittent, values for fluxes in very stable conditions. They produced empirical functions that fit their data (and the Kansas data) and do not result in a critical Richardson number, but lead to rapidly decreasing fluxes as stability increases. A preliminary analysis of tower data over sea ice in the Surface Heat Budget of the Arctic (SHEBA) experiment (Persson et al. 2002) has also found small but finite fluxes in very stable conditions. These small fluxes may be caused by breaking atmospheric gravity waves or some other process of nonshear-driven turbulence for which Monin–Obukov scaling is inappropriate. Pending more information, we adopt the Bejaars and Holtslag functions, which have eliminated occasional pathological results obtained with version 2.5.

b. Conservative moisture variables and the Webb et al. (1980) correction

By considering the conservation properties of the mixing ratio, r_x, of some scalar quantity with mass concentration, x, Webb et al. (1980) showed that the true interfacial flux can be represented as

$$\rho_a\overline{w'r_x'} = \overline{w'x'} + \left[\frac{m_a}{m_v}\frac{\overline{w'Q'}}{\rho_a} + \left(1 + \frac{m_a}{m_v}q\right)\frac{\overline{w'T'}}{T}\right]X = \overline{w'x'} + WX, \tag{14}$$

where ρ_a is the total density of air, m_a is the molecular weight of air and m_v the molecular weight of water vapor ($m_a/m_v = 1.61$), Q is the water vapor density, and W is the very small mean vertical velocity required to conserve mass because temperature and moisture affect the density of air:

$$W = \frac{m_a}{m_v}\frac{\overline{w'Q'}}{\rho_a} + \left(1 + \frac{m_a}{m_v}q\right)\frac{\overline{w'T'}}{T}. \tag{15}$$

Most observations of humidity fluxes and transfer coefficients are based on measurements of $\overline{w'Q'}$. Transfer coefficients are usually computed as

$$C_Q = \frac{\overline{w'Q'}}{S\Delta Q} \approx \frac{\overline{w'Q'}}{\rho_a S\Delta q}, \tag{16}$$

where $q = Q/\rho_a$. However, we can apply (14) to moisture flux (i.e., set $x = Q$) and then the actual latent heat cooling realized at the interface is derived from the con-

servative flux. Note that $q = r_Q/(1 + r_Q)$ and, because r_Q is typically on the order of 0.01, water vapor mixing ratio, r_Q, and specific humidity are essentially interchangeable. The COARE 2.5 algorithm represents this as

$$H_l = \rho_a L_e \left(\frac{\overline{w'Q'}}{\rho_a} + Wq \right) = \rho_a L_e (C_Q S \Delta q + Wq), \quad (17)$$

where C_Q was obtained by fits to the COARE measured flux data via (16) and the correction term is returned by the model. For version 3.0, the data were reanalyzed using the proper conservative quantity $\overline{w'r'_x}$:

$$C_e = \frac{\overline{w'Q'} + WQ}{\rho_a S \Delta q}. \quad (18)$$

Neglecting the small difference in moisture and heat transfer coefficients, we can show that C_Q and C_e are simply related

$$C_e = (1 + 1.61q)\left(1 + \frac{q}{T}\frac{\Delta\Theta}{\Delta q}\right) C_Q \quad (19a)$$

$$H_l = \rho_a L_e C_e S \Delta r_Q \approx \rho_a L_e C_e S \Delta q. \quad (19b)$$

Because C_e parameterizes the fundamentally conserved flux, we argue that it is the fundamental transfer coefficient and C_Q would, thus, depend not only on the ocean surface properties (i.e., the roughness lengths) but also on mean conditions as described by (19). The ratio C_e/C_Q will typically vary from 1.05 in the Tropics to 1.02 at high latitudes. Because we incorporate the Webb correction into our parameterization of C_e, our values are 2%–5% larger than conventional representations based on analysis of water vapor mass flux alone. The new version of the model computes $\overline{w'r'_Q}$ so (15) becomes

$$W = \frac{\frac{m_a}{m_\nu}\overline{w'r'_Q} + \left(1 + \frac{m_a}{m_\nu}q\right)\frac{\overline{w'T'}}{T}}{1 + \frac{m_a}{m_\nu}q}. \quad (20)$$

Here W is no longer needed for the moisture flux, but it can be used to compute Webb corrections for other trace gases where the basic measured quantity is mass concentration.

c. The Charnock parameter

As described in Fairall et al. (1996a) a range of values have been ascribed to the so-called Charnock constant, α, which appears in (6). For version 2.5 of the COARE algorithm we took $\alpha = 0.011$. This was the value suggested by Smith (1988), which also agreed with that obtained by direct measurement during COARE. By rearranging (4) and (6), and calculating neutral values at 10-m standard height,

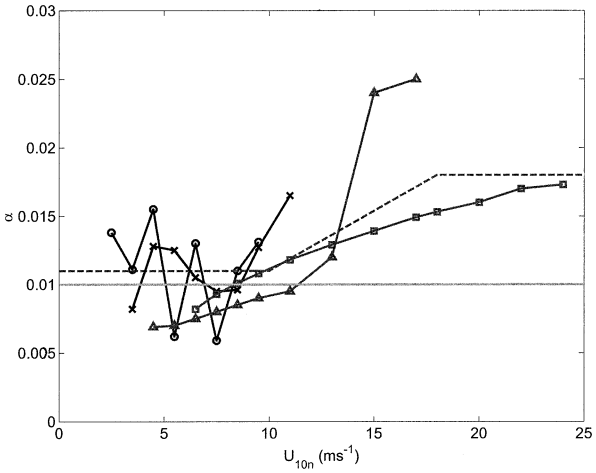

FIG. 1. Estimates of Charnock parameter from various field programs: ×, COARE; ○, SCOPE; △, MBL; □, Yelland and Taylor (1996). The dashed line is the COARE 3.0 relationship.

$$z_{o10n} = 10 \exp(-\kappa/c_{d10n}^{1/2}) \quad (21)$$

$$a = \left(z_{o10n} - \frac{0.11\nu}{u_*} \right) \frac{g}{u_*^2}. \quad (22)$$

However, COARE winds seldom exceeded 10 m s^{-1}; subsequent measurements in higher wind speed regions found larger values for α as wind speeds increased beyond 10 m s^{-1}. One key result that appeared in the literature (Yelland and Taylor 1996) was a substantial analysis of inertial-dissipation (ID; see the appendix) stress measurements for wind speeds between 6 and 26 m s^{-1}, which showed α increasing monotonically from 0.011 to 0.017. Covariance measurements by ETL and the Woods Hole Oceanographic Institution (WHOI) on R/V *Wecoma* off California during the Marine Boundary Layers (MBL) Experiment gave preliminary results with similar or even greater increases in α. Figure 1 shows measurements of α from several field campaigns that were available to us for the initial development of version 3.0 of the COARE algorithm. Based on this evidence, we adopted the form shown in Fig. 1, where α increases linearly from 0.011 at $U_{10n} = 10$ m s^{-1} to 0.018 at $U_{10n} = 18$ m s^{-1}, and remains constant for lack of better information beyond this wind speed.

Yelland and Taylor's (1996) results were a major factor in our decision to allow α to increase with wind speed above 10 m s^{-1}. Ironically, in more recent papers Yelland and Taylor have reanalyzed their ID-based flux estimates so that they no longer support the increase in α specified in COARE 3.0. Yelland et al. (1998) revised their 1996 results using corrections to mean winds and measurement heights from computational fluid dynamics (CFD) calculations on models of their ships. Another revision (Taylor and Yelland 2000) was made after adopting an improved dimensionless dissipation function to calculate their ID stress values. These changes have reduced their values for α to about 0.011 for all

wind speeds. Thus, the behavior of Charnock's parameter at wind speeds above 10 m s^{-1} remains controversial, and we will look to analysis of the large number of direct covariance and ID stress measurements that are accumulating in the ETL database to help resolve the matter. It is important because of the increasing application of bulk flux algorithms to severe storm situations.

d. Surface wave influence on roughness parameters

For wind speeds greater than about 5 m s^{-1}, surface waves are a dominant factor in the surface roughness of the ocean. A simple description of surface roughness such as (6) represents the average surface wave climate of an ensemble of measurements. If this is reasonably similar to that of the open ocean, then the results are useful in many applications. However, it is sometimes desirable to know the stress appropriate for the actual wave conditions, for example, in coastal regions where the wave climate is different from that of the open ocean (Gulev et al. 1998). Furthermore, if we knew more about the linkage between wave properties and surface roughness, measurements from diverse regions could be associated more rationally than by simple averaging. The literature abounds with analyses and models that address this issue, ranging from crude parameterizations based on the simplest wave properties (e.g., significant wave height or phase speed of the dominant waves) to complicated integrations based on the two-dimensional wave spectrum.

The original COARE bulk flux model did not consider wave conditions, primarily because no detailed wave measurements were made but also partly because the wave stress community lacked consensus on how to handle waves. Subsequently some progress has been made in this regard, although it is fair to say that consensus is still lacking. However, we have incorporated into COARE 3.0 two recent parameterizations, each of which allows the Charnock parameter or velocity roughness length to be calculated from specified wave properties.

The first relationship is from Taylor and Yelland (2001):

$$z_o = 1200 h_s (h_s/L_p)^{4.5}, \tag{23}$$

where h_s is the significant wave height (mean height of the upper third of the height distribution that is approximately 4 times the rms surface elevation at a point) and L_p the wavelength associated with the peak of the wave frequency–size spectrum (the so-called dominant wave period, T_p). Therefore h_s/L_p is approximately the slope of the dominant waves. The coefficients are purely empirical, and are based on fits to extensive observations by Taylor, Yelland, and colleagues plus several sets of data from other experiments (including shallow water). The second relationship is from Oost et al. (2002):

$$\alpha = 50(C_p/u_*)^{-2.5}, \tag{24}$$

where C_p is the phase speed of the dominant wave and C_p/u_* is a measure of ''wave age'' (wave age is sometimes also defined as C_p/U_{10}). This result is based entirely on data obtained in several campaigns at the Dutch research platform in the North Sea.

To implement these relationships in COARE 3.0 we have rewritten (24) in terms of roughness, and added the smooth flow component to each

$$z_{oTY} = 1200 h_s (h_s/L_p)^{4.5} + 0.11\nu/u_* \tag{25a}$$

$$z_{oOe} = \frac{50}{2\pi} L_p (u_*/C_p)^{4.5} + 0.11\nu/u_*. \tag{25b}$$

The similarity of the relationships is interesting although the fact that they have the same power-law dependence is almost certainly a coincidence.

COARE 2.5 represented the average wave–roughness relationship through (6) with a constant Charnock parameter, $\alpha = 0.011$. COARE 3.0 specifies α to increase slightly with wind speed in the 12–18-m s^{-1} range as described above, and is provided with a switch so that the user can choose between the average Charnock relation or either of these two wave parameterizations. With (25a) one must provide significant wave height and wave period; with (25b) only wave period is required. The relevant parameters are computed in the model using standard deep-water gravity wave relationships:

$$L_p = \frac{gT_p^2}{2\pi}; \qquad C_p = \frac{gT_p}{2\pi}. \tag{26}$$

These options may enable users to assess potential wave-induced uncertainties in the flux results. They are offered in the model without critical comment except to note that they were produced by two different experimental groups with well-deserved reputations for careful and thoughtful measurements and analysis. Figure 2 shows a comparison of the neutral momentum transfer coefficient for fully developed seas using the three COARE 3.0 options and the measurements of Smith (1980). We use the formulas for fully developed sea given by Taylor and Yelland (2001):

$$h_s = 0.0248 U_{10n}^2; \qquad T_p = 0.729 U_{10n}. \tag{27}$$

Note that (27) is equivalent to $C_p/U_{10n} = 1.14$; some wave practitioners prefer to specify fully developed conditions in terms of $C_p/u_* \approx 28$.

We cannot claim that the wave climate of the dataset used to develop COARE 3.0 is, on average, well developed at all wind speeds, so Fig. 2 does not imply that one model is better than the other. The duration/fetch required to reach the fully developed state increases with mean wind speed, so it seems likely that well-developed conditions are more commonly observed at moderate winds. However, this issue is confused by possible contributions to the stress of swell

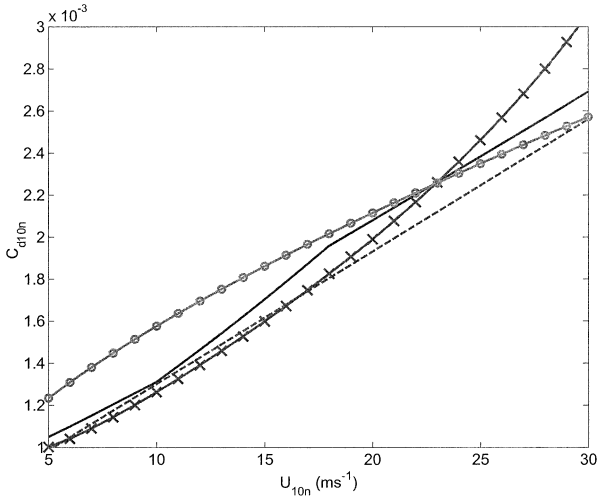

FIG. 2. Wind speed dependence of the 10-m neutral momentum transfer coefficient from several sources: solid line, COARE 3.0; dashed line, Smith (1980); line with ×, Oost et al. (2002) parameterization for fully developed seas; line with ○, Taylor and Yelland (2001) parameterization for fully developed seas.

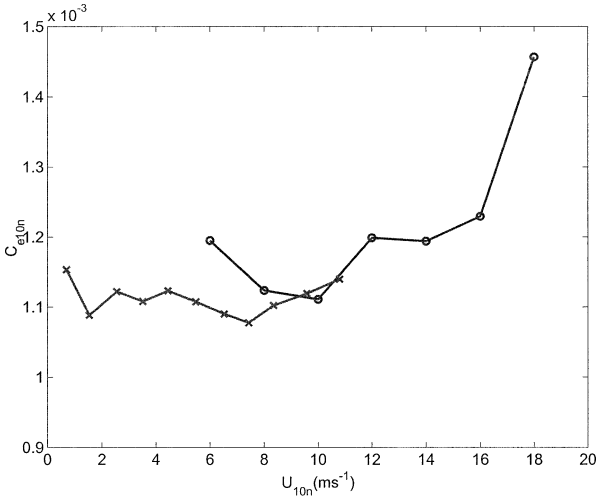

FIG. 3. Wind speed dependence of the 10-m neutral humidity transfer coefficient from the COARE-plus dataset (line with ×) and modified values from the HEXMAX program (line with ○).

waves that are not associated with the local winds; this becomes increasingly significant at low wind speeds and/or in high wind regions where larger swell is more common.

e. Scalar roughness length parameterization

LKB (and COARE 2.5) parameterized the scalar roughness Reynolds numbers in terms of R_r [Eq. (7)], based on sublayer transfer and surface renewal theory, supported with a limited amount of field data. To produce the new scalar roughness parameterization for COARE 3.0, we combined some ETL datasets (see section 4) and added a reanalysis of data from HEXOS conducted on the Dutch tower in the North Sea (Smith et al. 1996). The COARE measurements on R/V *Moana Wave* produced about 850 h of usable humidity flux data. We focus on the behavior of moisture parameters, because the range of latent heat flux is much greater than that for sensible heat in our datasets, and historically it has received the greater attention. Data from two field programs prior to COARE [the Tropical Instability Wave Experiment (TIWE) and the Atlantic Stratocumulus Transition Experiment (ASTEX)] and one subsequent to COARE [the San Clemente Ocean Probing Experiment (SCOPE)] provided an additional 450 usable values. All measurements in this combined set, which we call COARE-plus, were made with the same system and processing methods. The SCOPE data were obtained from R/P *FLIP* which, because of minimal motion and flow distortion, are of unusually high quality and consistency (Grachev and Fairall 1997). The fluxes and bulk variables were averaged in 10-m neutral wind speed bins, and transfer coefficients were computed. This analysis gave a reasonably clean depiction of the wind speed dependence of C_{e10n} for U between 0 and 10 m s^{-1}.

For the higher wind speed regime, we used published results (DeCosmo et al. 1996) from HEXMAX. To make the HEXMAX transfer coefficients consistent with our COARE-plus data, they were modified to account for the cool skin (the cooler interface implies lower water vapor pressure, so that a larger transfer coefficient is required to produce the observed flux), the 2% reduction in water vapor pressure over seawater, and the Webb et al. (1980) correction. These changes increased their transfer coefficients by about 8%; the DeCosmo et al. (1996) *median* values were used to reduce the sensitivity to outliers and a skewed distribution. The maximum wind speed for usable humidity data from HEXMAX was about 18 m s^{-1}. The two datasets are shown in Fig. 3 as a function of wind speed. Because the HEXMAX conditions were much rougher than typical open ocean regions at the same wind speed, we have converted the results to roughness Reynolds number, R_r, which we take to be a more fundamental representation of air–sea surface interaction properties than the wind speed; these results are shown in Fig. 4. The compatibility of the ship-based, primarily tropical data with the platform-based, North Sea data is striking and encouraging.

The LKB polynomial relationships were presented in lookup tables and took slightly different forms for R_t and R_q, so that the scalar roughness lengths and therefore the transfer coefficients were different. The behavior of z_{oq} with R_r shown in Fig. 4 offers a much simpler mathematical relationship than LKB to represent (7). We, therefore, adopt the following empirical fit to the COARE-plus and HEXOS data:

$$z_{oq} = \min(1.1 \times 10^{-4}, 5.5 \times 10^{-5} R_r^{-0.6}), \quad (28)$$

which is shown in Fig. 4, and take the same relationship

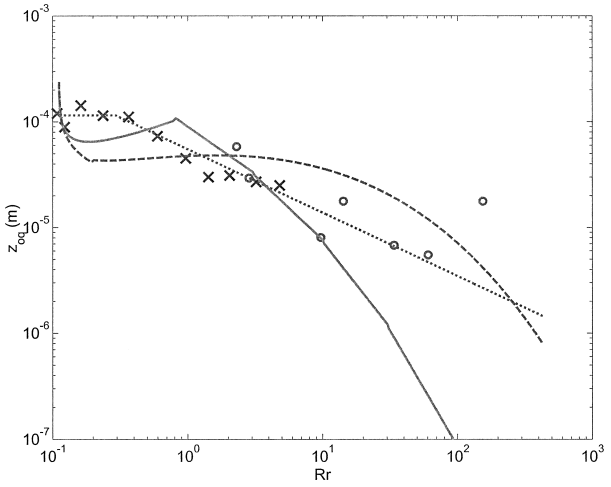

FIG. 4. Roughness Reynolds number dependence of the humidity transfer roughness length: ×, COARE-plus; ○, modified HEXMAX; solid line, LKB model (COARE 2.5); dashed line, Brutsaert–Garratt parameterization; dotted line, COARE 3.0.

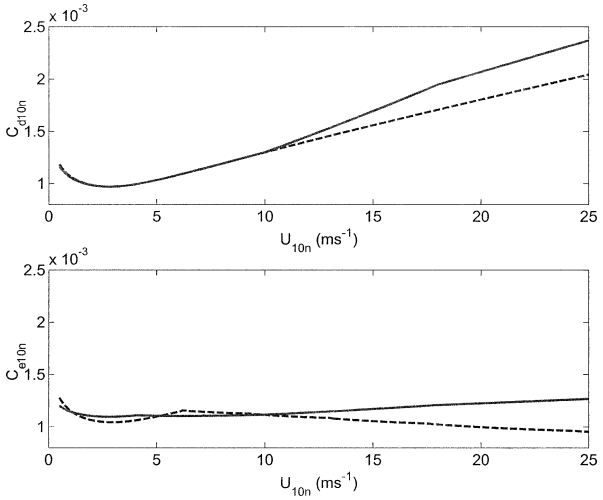

FIG. 5. Wind speed dependence of the momentum and scalar transfer coefficients for COARE versions 2.5 (broken line) and 3.0 (solid line): (top) C_{d10n}; (bottom) C_{e10n}.

for z_{ol}. Also shown in Fig. 4 are the original LKB (=COARE 2.5) parameterization and a parameterization from Garratt (1992), based on the surface renewal approach of Brutsaert (1975), where z_{oq} is given as

$$z_{oq} = z_o \exp(2 - 2.28R_r^{1/4}). \quad (29)$$

When translated into C_{e10n}, the differences between the three models would be difficult to distinguish in a few 1-month field campaigns. The decrease of z_{oq} with R_r (or wind speed) is usually attributed to the relatively increasing importance of the molecular transfer bottleneck near the interface; momentum transfer has an additional transfer mechanism due to pressure and does not exhibit this behavior. Figure 5 shows version 2.5 and 3.0 neutral exchange coefficients as a function of wind speed. Beyond 10 m s^{-1} COARE 2.5 is a pure extrapolation, with no validation.

4. Flux and transfer coefficient evaluation

Table 2 lists the series of 12 deployments of the ETL seagoing flux system, beginning before the COARE field program and ending in late 1999. The basic flux measuring system and software (see the appendix) remained essentially the same but sensor models, data acquisition structure, computers, etc., were upgraded over the period. As described in section 3e, data from the first six cruises formed the COARE-plus database. Because this contained only 67 h of data at wind speed greater than 10 m s^{-1}, it was augmented with 94 h of HEXMAX data and used to formulate COARE 3.0. Data from the six later cruises have been combined with the first six to form a larger database (ETL1999) containing 7216 h of data, including about 800 h with wind speeds exceeding 10 m s^{-1} and 2200 h at high latitudes. This

TABLE 2. Summary of ETL air–sea flux and bulk meteorological data cruises used in the analysis: Tropical Instability Wave Experiment (TIWE); Atlantic Stratocumulus Transition Experiment (ASTEX); Coupled Ocean–Atmosphere Response Experiment (COARE); San Clemente Ocean Probing Experiment (SCOPE); Fronts and Atlantic Storms (FASTEX); Joint Air–Sea Monsoon Experiment (JASMINE); Nauru '99 Experiment (NAURU99); Tropical Rainfall Measuring Mission (TRMM)/Kwajalein Experiment (KWAJEX); Pan American Climate Studies fall 1999 study (PACSF99).

Cruise name	Dates	Hours	Vessel	Lat	Lon	Reference
TIWE	21 Nov–13 Dec 1991	460	*Moana Wave*	0°	140°W	Chertock et al. (1993)
ASTEX	6–28 Jun 1992	390	*M. Baldrige*	30°N	25°W	White et al. (1995)
COARE-1	11 Nov–3 Dec 1992	589	*Moana Wave*	2°S	156°E	Fairall et al. (1996)
COARE-2	17 Dec 1992–11 Jan 1993	648	*Moana Wave*	2°S	156°E	Fairall et al. (1996)
COARE-3	28 Jan–16 Feb 1993	385	*Moana Wave*	2°S	156°E	Fairall et al. (1996)
SCOPE	17–28 Sep 1993	305	*FLIP*	33°N	118°W	Edson and Fairall (1998)
FASTEX	23 Dec 1996–24 Jan 1997	730	*Knorr*	45°N	10°–60°W	Hare et al. (1999)
JASMINE	5–31 May 1999	654	*Ron Brown*	8°N	89°E	Fairall et al. (2000)
NAURU99	15 Jun–18 Jul 199	794	*Ron Brown*	0.5°S	167°E	Fairall et al. (2001)
KWAJEX	28 Jul–12 Sep 1999	875	*Ron Brown*	8°N	167.5°E	None
Moorings	14 Sep–21 Oct 1999	746	*Ron Brown*	52°N	140°W	None
PACSF99	11 Nov–2 Dec 1999	640	*Ron Brown*	±10°N	100°W	None

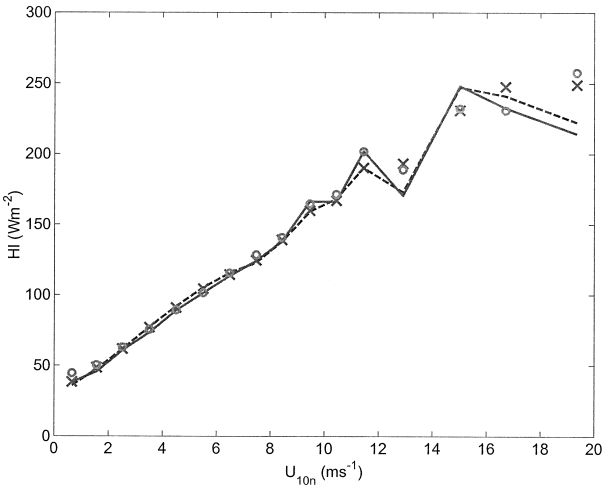

FIG. 6. The average of covariance and ID latent heat fluxes computed in 10-m neutral wind speed bins. Mean values are shown by lines and medians by symbols: the solid line and circles are measured fluxes, and the broken line and crosses are calculated with COARE 3.0.

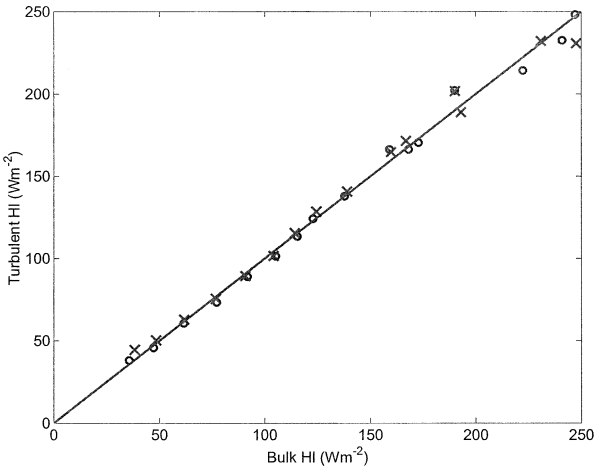

FIG. 7. The same data points from Fig. 6, but plotted as bulk latent heat flux vs measured turbulent values. The × symbols are the means; the ○ symbols are medians; the solid line is 1:1.

allows us to test the algorithm over the wind speed range from 0 to 20 m s^{-1}.

We first scan the database to select a subset of covariance and ID flux estimates that satisfy criteria designed to reject invalid or unreliable points. The criteria include experimental aspects (e.g., relative wind direction within a certain sector to avoid interference by the ship's structure), instrument performance indicators, avoidance of ship maneuvers, and requirements that certain variables (e.g., variances) fall within physically reasonable limits. We might reject a specific flux value if the standard deviation of wind speed normalized by the mean wind speed exceeded some limit, but never reject a flux value based on its comparison with the bulk model. At sea, the shipboard system records continuously, irrespective of weather or operational conditions, so that such quality controls are needed to ensure a dataset that is clean, coherent, and relevant to the geophysical problem under investigation. In the present case, 4946 h for stress and 4276 h for latent heat flux were accepted (covariance, ID, and bulk).

The next step is to compare the values of fluxes obtained from the bulk algorithm with the measurements in some rational fashion. Usually we are interested in the average performance of the bulk algorithm, with information on its statistical scatter about the observations. In this analysis we show comparisons of quantities averaged in bins of 10-m neutral wind speed with the additional condition that the air–sea specific humidity difference exceeds 2.0 g kg^{-1}. Figure 6 shows such a comparison for latent heat flux. The bin width increases slightly at the data-sparse higher wind speeds; bins with fewer than five values are not shown. The turbulence values are the average of covariance and ID values; the bulk values are COARE 3.0. We plot both medians and means to reveal skewed distributions or effects of outliers. Figure 7 shows these same values plotted on an *x*–*y* linear scale. Figure 8 shows a similar comparison for stress, using only medians and averaging the covariance and ID values separately.

Figures 7 and 8 indicate very close agreement between model and data, but a more critical test comes with the evaluation of transfer coefficients (2). The experimental determination of transfer coefficients is difficult, because turbulent flux data are inherently noisy and bulk meteorological quantities difficult to measure with sufficient accuracy. From (2) and (4) we can compute a 10-m neutral transfer coefficient for each observation,

$$C_{x10n} = \frac{\overline{w'x'}}{U_{10n}\Delta X_{10n}G}, \tag{30}$$

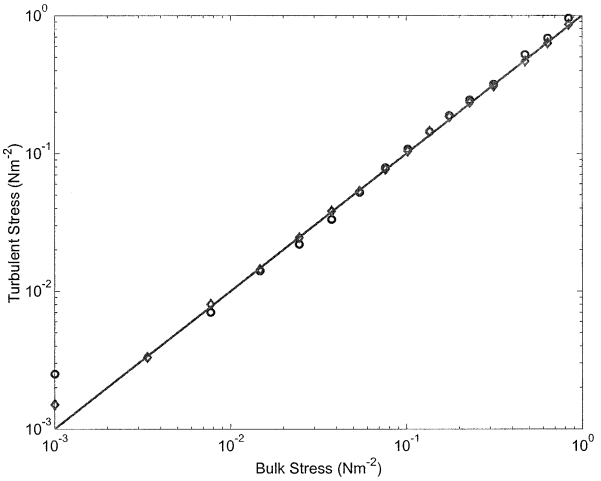

FIG. 8. As in Fig. 7 but for median turbulent stress. The ○ symbols are the covariance values; the ◊ symbols are the ID values.

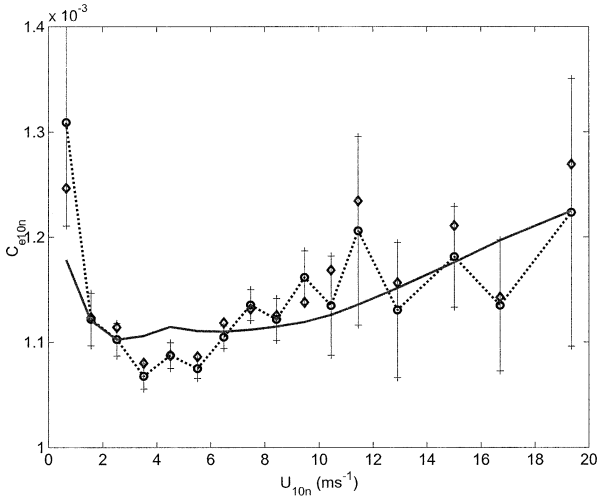

FIG. 9. The 10-m neutral transfer coefficient for moisture (○), calculated with Eq. (33) and using the average of mean and median values, as a function of the 10-m neutral wind. Error bars indicate the statistical uncertainty (one sigma) of the bin-average based on the distribution within the wind speed bin. The heavy solid line is COARE 3.0. The ◊ symbols are computed with the SM (see text) using the median values.

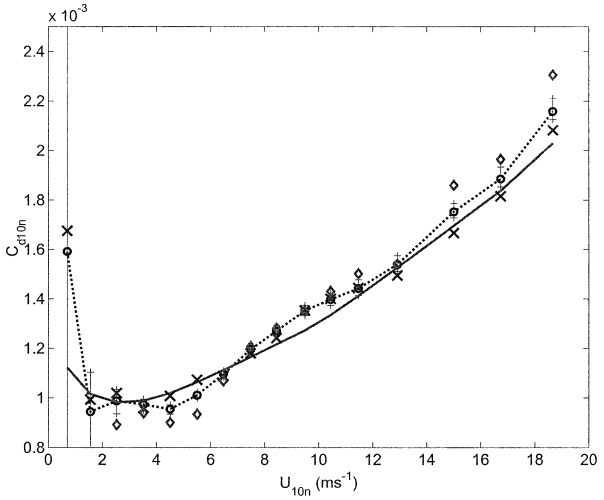

FIG. 10. Median 10-m neutral velocity transfer coefficient as a function of 10-m neutral wind using method 3 [Eq. (33)]. Error bars indicate the statistical uncertainty (one sigma) of the bin median based on the distribution within the mean wind speed bin: ○, combined covariance and ID values; ×, ID values only; ◊, covariance values only.

where $G = S/U$ is the gustiness factor and, for simplicity, we assume $V = 0$. The 10-m neutral wind is computed from the wind measured at height z as

$$U_{10n} \equiv \frac{u_*}{\kappa G^{1/2}} \ln\left(\frac{10}{z_o}\right) = U(z) - \frac{u_*}{\kappa G^{1/2}}\left[\ln\left(\frac{z}{10}\right) - \psi_u(\zeta)\right], \quad (31)$$

and the 10-m air–sea humidity difference is

$$\Delta q_{10n} = \Delta q(z) + \frac{q_*}{\kappa}\left[\ln\left(\frac{z}{10}\right) - \psi_q(\zeta)\right]. \quad (32)$$

To reduce sampling noise and avoid artificial correlations, we use bulk-derived values of MOST scaling parameters to compute the neutral 10-m values.

There are several ways in which average transfer coefficients may be computed for each wind speed bin. Simply using bin-average values of the individual quantities in (30) is subject to errors due to nonlinearity in stability effects and is therefore avoided. The straightforward method (SM) is to calculate (30) for each 1-h observation within each wind speed bin, then average. This eliminates the nonlinearities but is sensitive to cross talk between errors in the individual terms, outliers, and small errors unless a median is used. We have experimented with several other approaches, and find that the scheme given in (33) best reduces variability in the average transfer coefficients:

$$\langle C_{x10n}\rangle_3 = \frac{\langle\overline{w'x'}\rangle}{\langle\overline{w'x'}\rangle_b}\langle C_{x10nb}\rangle. \quad (33)$$

The bulk algorithm is used to compute bulk fluxes and transfer coefficients that are then averaged in each bin. The required transfer coefficient is the mean bulk coefficient multiplied by the ratio of mean measured to mean computed (bulk) fluxes. If the bulk model is reasonably accurate, (33) yields the transfer coefficient associated with the *measured* average flux.

In Fig. 9 we show the comparison between measured and modeled C_{e10p} using (33) and the average of mean and median values (we also show results of the SM using medians). The rms deviation of these values from the model is 4.0%. The statistical uncertainty in the mean 10-m neutral transfer coefficients, shown as error bars, was estimated by dividing the standard deviation of points within each wind speed bin, σ_{C_e}, by the square root of the number of observations in the bin.

Corresponding results for the momentum transfer coefficient are shown in Fig. 10, where again the error bars correspond to the uncertainty in the estimates. Figure 11 shows the Charnock parameter computed from the transfer coefficients given in Fig. 10 using (21) and (22). The large amount of new data at higher wind speeds strongly support the increasing α built into COARE 3.0 on the evidence of Fig. 1, and suggest that it continues to increase beyond 18 m s^{-1}. The comparison is not valid below 5 m s^{-1} because z_o approaches the smooth flow limit 0.11 ν/u_*.

In Fig. 12 the results shown in Fig. 9 have been converted to moisture roughness lengths and superimposed on those in Fig. 4. At low wind speeds, the values for z_{oq} and R_r are quite sensitive to the method used to obtain z_o and u_*, and confused by the contributions of swell, which are not accounted for in MOST. Apart from the highest and lowest wind speeds, agreement between

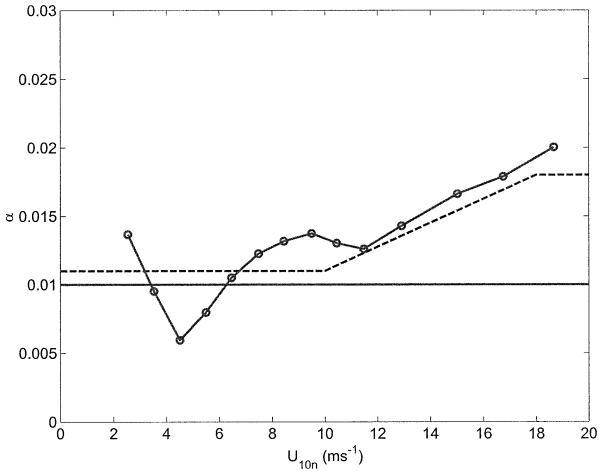

FIG. 11. Charnock parameter as a function of 10-m neutral wind using the mean turbulence values (○) from Fig. 10. The dashed line is COARE 3.0; the solid straight line a value of 0.01.

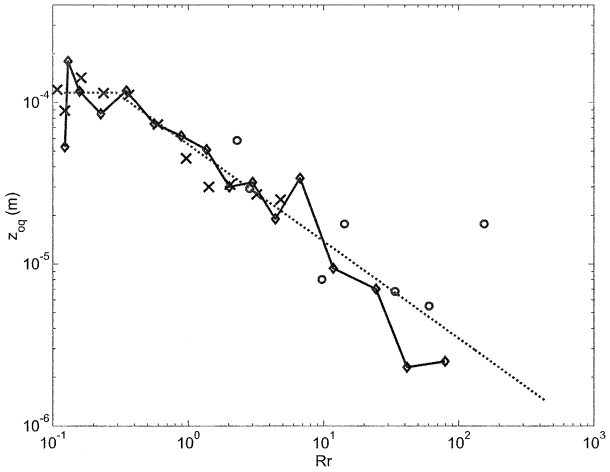

FIG. 12. Moisture roughness length as a function of the roughness Reynolds number, as in Fig. 4 but showing the relation of ETL1999 (◇) to COARE 3.0 [dotted line, Eq. (28)]. COARE-plus data shown as × and modified HEXMAX as ○.

COARE 3.0 and the measurements is excellent, and noticeably better than that shown in Fig. 9. This reflects the compensating effect of deviations of C_{d10n} from the model, as shown in Fig. 10, on measured C_{e10n}, since

$$z_{oq} = 10 \exp\left(-\kappa \frac{C_{d10n}^{1/2}}{C_{e10n}}\right). \quad (34)$$

Figure 13 shows R_q as a function of R_r. Again, the model fits the ETL1999 measurements well. The original Garratt–Brutsaert model, referred to in section 3e and Fig. 4, fits poorly, but becomes a good fit with slight change of parameters:

$$R_q = R_r \exp(3.4 - 3.5R_r^{1/4}). \quad (35)$$

Since the total variation of R_q is relatively small over the range of R_r from 0.1 to 100, a two-parameter fit is adequate.

5. Discussion

Here we compare the results presented above with previous measurements of air–sea exchange coefficients. There have been several recent comparisons of flux algorithms (CFC; ZZD; Chang and Grossman 1999) that showed that for $U < 10$ m s^{-1} results agreed quite closely, but diverged at higher wind speeds. However, few quality observations for $U > 10$ m s^{-1} existed to validate these comparisons. Shallow-water observations (e.g., HEXMAX) require some physical model to relate to open-ocean conditions. For stress, a consensus model is presently lacking; for scalar transfers we use roughness Reynolds number similarity, as described in the previous section. The new results presented in this paper, for air–sea fluxes and exchange coefficients, and on which the revised COARE bulk algorithm is based, derive from a very large database (ETL1999). The total number of hours of observation used in this study significantly exceeds the total number considered in previous reviews. They also benefit from great advances in sensor and computational technology as described in the appendix.

In Fig. 9, the increase in C_{e10n} toward very low wind speeds confirms, with about 700 h of data below 2.5 m s^{-1}, the behavior observed by Bradley et al. (1991) and embodied in LKB and both versions 2.5 and 3.0 of the COARE algorithm. For wind speeds above 4 m s^{-1}, previous estimates of C_{e10n} are usually given as a constant value because the accuracy ascribed to the measurements does not warrant more detail. The review by Smith (1989) found $C_{e10n} = 1.2\ (\pm 0.1) \times 10^{-3}$ for winds

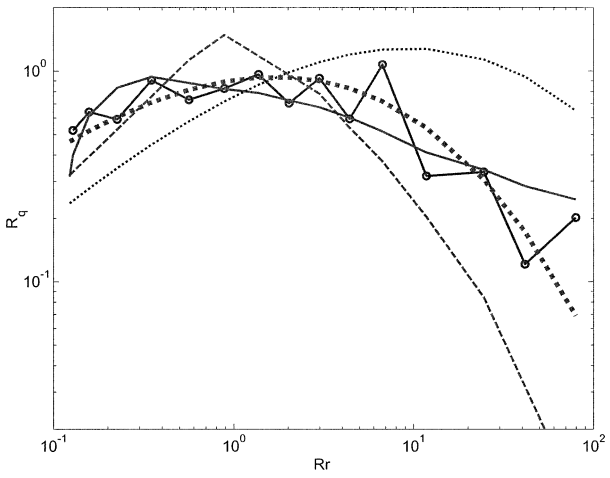

FIG. 13. Humidity roughness Reynolds number vs velocity roughness Reynolds number: ○, ETL1999 dataset results; solid line COARE 3.0 [Eq. (28)]; dashed line LKB and COARE 2.5; dotted line, Garratt–Brutsaert [Eq. (29)]; heavy dotted line, revised Garratt–Brutsaert [Eq. (35)].

from 4 to 14 m s^{-1}; Garratt (1992) and Smith et al. (1996) quote 1.1×10^{-3} ±15% for winds between 3 and 20 m s^{-1}; for the HEXMAX data DeCosmo et al. (1996) give 1.1×10^{-3} and find no significant variation with wind speed up to 18 m s^{-1}. To compare with these, we calculate the constant value for C_{e10n} which fits the data above 5 m s^{-1}, and find 1.15×10^{-3} within 5.3%. This value may not compare directly because it includes the following: 1) reduction in seawater vapor pressure by 2% due to salinity, 2) a true air–water interface temperature (i.e., cool skin corrected), and 3) the Webb et al. correction. These factors combine to increase the mean moisture transfer coefficient by more than 6%.

However, as shown in Fig. 9, both the early data used to tune COARE 3.0 and the large ETL1999 database clearly demonstrate that C_{e10n} increases steadily toward higher winds. Previously, the HEXMAX data were the most significant high wind speed results for the moisture transfer coefficient. After adjustment as described in section 3e, HEXMAX is consistent with our measurements, whether graphed as C_{e10n} versus wind speed or z_{oq} versus R_r.

The neutral drag coefficient is well known to increase with wind speed and is often given an empirical linear form above about 5 m s^{-1} (e.g., Garratt 1992; Smith 1980; Yelland et al. 1998). The ETL1999 data in Fig. 10 confirm that a linear representation is not unreasonable, but is less enlightening than a model based on the physical concepts of air–sea exchange described in section 2. The Smith (1988) model embodied in COARE 3.0, Eq. (6), predicts an increase in C_{d10n} toward low wind speeds. As shown in both the covariance and ID measurements in Fig. 10, only for wind speeds less than about 1 m s^{-1}, does C_{d10n} increase above its minimum value of about 1.0×10^{-3}, which appears constant to about 5 m s^{-1}. Between about 6 and 14 m s^{-1}, the ID values are on average 3.0% lower than the covariance values, but the difference increases above 15 m s^{-1}. Agreement between COARE 3.0 and combined ID and covariance 10-m neutral drag coefficients is about 4%. In fact, the ID values for stress and drag coefficient agree closely with the model, while the covariance values tend to be higher at high wind speed and slightly lower at low wind speed. Covariance could be overestimated by about 10% because of ship flow distortion; the ID results could be underestimated by a similar amount because of loss of pressure transport production of turbulent kinetic energy (TKE) to the growing waves (Janssen 1999).

Most of our measurements for $U > 12$ m s^{-1} were acquired in the Fronts and Atlantic Storms Experiment (FASTEX) (North Atlantic) and Moorings (North Pacific) field studies and the number of useable observations for $U > 15$ m s^{-1} is fairly small (133 h for stress; 85 h for moisture). In the high wind regime, our drag coefficient values are somewhat higher than those of Smith (1980) and Taylor and Yelland (2000). For simplicity, consider values of $10^3 C_{d10n}$ at $U = 20$ m s^{-1}: Smith, 1.93; Taylor and Yelland, 1.92; this dataset, covariance, 2.30 and ID, 2.07. The average of these four values is 2.06 and the spread is from +12% to −7%. Part of the difference between our ID result and that of Taylor and Yelland lies in the choice of dimensionless dissipation function. A change in Kolmogorov constant from 0.55 to 0.53 [the value consistent with Edson and Fairall (1998, hereafter referred to as EF)] would increase the Taylor and Yelland neutral transfer coefficient by 3.8% to 1.99. The COARE 3.0 value at 20 m s^{-1} is 2.06. Overall, we estimate that the COARE 3.0 transfer coefficients when applied to 1-h bulk measurements over the open ocean are accurate to about 5% for wind speeds 0–10 m s^{-1} and better than 10% for 10–20 m s^{-1}.

In the wind speed range 0–20 m s^{-1} the major remaining surface physics issue is the influence of surface waves on the fluxes. With present techniques, a huge number of observations will be required to obtain definitive results because of the addition of one or two independent variables. High-quality, routine measurements of wave properties is an important technical challenge, so we must hope for a breakthrough in theory or modeling. A second major issue is the application of our measurement-based algorithms in numerical models. One aspect is the difference between one-dimensional and two-dimensional representations (Vickers and Esbensen 1998) but most of the problems are associated with resolved versus unresolved (subgrid scale) processes and variability. The COARE algorithm accounts for velocity variability caused by boundary layer–scale eddies, but that is the only unresolved process explicitly in the model. Of course, when the model is applied to point measurements of the appropriate timescale, other sources of variability are explicitly resolved by the input data. In many numerical models moist convective processes are at least partly unresolved and this is a large source of variability. Some investigators (Jabouille et al. 1996; Zulauf and Krueger 1997; Redelsperger et al. 2000; Zeng et al. 2002) have tried adding a second gustiness velocity term, based on convective mass flux or precipitation rate, to the boundary layer convection-driven gustiness velocity (8). These studies used high-resolution models to simulate convective variability and examined the effect of spatial–temporal averages on the bulk flux relationships. The results have been encouraging but observational verification with conventional flux measurements is not straightforward. Rainfall studies encounter sampling problems and a point measurement of rainfall is a poor indicator of convective activity (at sea one can be surrounded by rainstorms for days and not collect any rain at the ship). Aircraft and ship-based scanning radars may be well suited to attack this problem.

The above analysis has ignored the possible effects of sea spray droplets on the moisture transfer coefficient. Our measurements of water vapor flux do not differentiate between evaporation from the sea surface and subsequent evaporation from sea spray droplets below

(or above) the sensors. Such effects are expected to become significant at winds exceeding 15–20 m s^{-1}, but production of spray droplets as a function of wind speed are still uncertain (Andreas et al. 1995) and the threshold for measurable effects is not known. Recent model studies (Pattison and Belcher 1999; Andreas 2001) suggest droplet effects on the order of 10 W m^{-2} for HEXOS-type conditions where direct evaporation is about 250 W m^{-2}. In our opinion, such models are not yet sufficiently accurate to justify their inclusion in COARE 3.0.

6. Conclusions

The COARE bulk flux algorithm has been updated and its range of wind speed validity is extended to 0–20 m s^{-1}; we designate this version COARE 3.0. The updates include improvements to the stability functions, shortening the stability iteration, and eliminating the need for a Webb correction to latent heat flux. The wind speed dependence of both velocity and scalar transfer coefficients is changed slightly, particularly above 10 m s^{-1}. The modifications were based on nearly 2800 h of direct flux measurements during six ETL cruises in the COARE era (referred to as COARE-plus), augmented with about 100 h of data at wind speeds above 10 m s^{-1} from the HEXMAX experiment. Neutral moisture exchange coefficients from the two data sources merged extremely well after the published HEXMAX results were adjusted for three established correction factors.

In LKB and COARE 2.5, the scalar exchange coefficients were based on a relationship between scalar and velocity surface roughness Reynolds numbers. Analysis of the combined dataset suggested a much simpler mathematical relationship for COARE 3.0, directly relating the scalar roughness length to roughness Reynolds number. The drag coefficient was changed via a revised Charnock constant, which increases above 10 m s^{-1} on the evidence of observations from several sources, including some of the COARE-plus cruises.

Flux measurements from six later cruises (1997–99) have been added to COARE-plus to form a very large air–sea interaction database (ETL1999). ETL1999 contains about 7200 h of direct covariance and inertial-dissipation flux observations, 800 h for wind speeds greater than 10 m s^{-1} and 2200 h outside the Tropics, as well as concurrent measurements of bulk meteorological, radiation, and ocean variables. When sorted into wind speed bins of about 1-m s^{-1} width, the average latent heat flux ranges from 40 to 250 W m^{-2} and average stress from 0.001 to 1.0 N m^{-2}. The large number of observations in the database removes most of the statistical uncertainty in determining the mean fluxes and transfer coefficients. There is much more data than previously existed for both high (>10 m s^{-1}) and low winds (<2 m s^{-1}). When subjected to quality control filters, there remain about 4500 direct flux observations of very high quality for research and validation purposes, including here the evaluation of COARE 3.0.

The observations in ETL1999 strongly support new relationships built into the revised algorithm, for the scalar roughness length dependence on roughness Reynolds number (Fig. 12) and the Charnock parameter, α (Fig. 11). Our combined covariance and ID measurements indicate α constant at 0.011 up to about 10 m s^{-1}, increasing thereafter to about 0.020 at 19 m s^{-1}.

On the basis that C_{e10n} is often represented as a constant value between 5 and 20 m s^{-1}, our analysis indicates a value 1.15×10^{-3}, close to several other recent determinations. However, our measurements clearly indicate that C_{e10n} increases steadily with wind speed from about 1.08×10^{-3} at 5 m s^{-1} to 1.2×10^{-3} at 18 m s^{-1}. COARE 3.0 fits these bin-averaged measurements with an rms deviation of 4.0%. The measured C_{d10n} values increase from about 1.0×10^{-3} at 3 m s^{-1} to 2.30×10^{-3} at 20 m s^{-1} if covariance fluxes are used, or 2.07×10^{-3} for ID fluxes. The difference may be partly due to flow distortion effects on the covariance values, and above 15 m s^{-1} a possible indication of the wave-pressure effects on TKE dissipation and hence ID estimates (Janssen 1999). The average of 2.18×10^{-3} is significantly larger (i.e., separated by several standard deviations) than the classic covariance measurements of Smith (1980) and the large ID database of Taylor and Yelland (2000). The COARE 3.0 value at 20 m s^{-1} is 2.06. For wind speed greater than 2 m s^{-1} it fits the combined covariance and ID measurements of C_{d10n} within 4.2%. At low wind speeds both C_{e10n} and C_{d10n} increase toward lower wind speeds as has been observed previously.

Two alternative wave parameterizations (Taylor and Yelland 2001; Oost et al. 2002) have been incorporated into COARE 3.0, to enable wave conditions to be used in the calculation of surface roughness. The purpose is to enable the algorithm to be applied in regions, such as the coastal zone, where the wave climate is different from the open ocean. This option has not been evaluated by the authors, for lack of detailed wave data. However, we hope that this capability will encourage users to apply the arcane field of wind–wave relationships to practical situations where wave measurements are available, and thereby advance this area of study.

Twenty years ago, a survey of bulk flux schemes by Blanc (1985) found 30% differences in moisture and momentum transfer coefficients at moderate wind speeds with major problems noted at low and high wind speeds. With advancements in technology, air–sea flux measurements from ships are being made almost routinely by several research groups around the world and the progress has been impressive. Extensive low wind speed measurements in the COARE program and the adoption of gustiness have significantly improved the situation for light winds. We submit that, when applied to 1-h bulk measurements over the open ocean, the COARE 3.0 transfer coefficients are accurate to about

5% for wind speeds 0–10 m s^{-1}. There is still need to resolve differences in the 10–20 m s^{-1} regime, but since Blanc's review these differences have reduced to around 10%. At the highest wind speeds the effects of spray have yet to be satisfactorily quantified. The issue of the effects of flow distortion on fluxes, particularly stress, still needs to be addressed through a combination of numerical, laboratory, and field studies. The great advancement in ship-based covariance measurements is highlighted by recent results on air–sea gas transfer where direct measurements of CO_2 fluxes and transfer velocity have been made (Fairall et al. 2000; McGillis et al. 2001). Until recently, such measurements were considered to range from the unacceptable to the impossible (Csanady 2001).

Acknowledgments. This work was supported by the ONR Marine Meteorology program, the DOE Atmospheric Radiation Measurement program, the NOAA Office of Global Programs, the National Science Foundation Climate Dynamics program, and Grant ATM-9727054 from NSF's Mesoscale Dynamics Meteorology program. The authors especially thank Scott Abbott, Dave Costa, Jesse Leach, Cat Russell, Dan Gottas, Jim Jordan, and Dave Gregg for their work, dedication, and personal sacrifice beyond all reason. Numerous discussions with Drs. Peter K. Taylor (SOC), Ed Andreas (CRREL), and Meghan Cronin (NOAA/PMEL) are gratefully acknowledged.

APPENDIX

The ETL Shipboard Flux Measuring System

The ETL seagoing flux and bulk meteorology measurement system was fully described in Fairall et al. (1997). The following deals with specific aspects relevant to computing bulk transfer coefficients.

a. Instruments

The basic measurements used in this paper are covariance and inertial-dissipation turbulent flux estimates, combined with measurements of the basic bulk variables as described in section 2. A sonic anemometer (Gill/INUSA RS-2 or RS-2A) is used to obtain the three components of the wind vector (u', v', w') and the sonic temperature (T'). A high-speed infrared hygrometer (Ophir Corporation IR-2000) is used to obtain Q'. Velocity fluctuations in fixed-earth coordinates are obtained from the raw anemometer output by applying rotations to account for pitch, roll, and yaw plus corrections for the ship's velocity vector. High-frequency (i.e., surface wave–induced) motions are measured with an integrated package of angular rate sensors and accelerometers (Systron Donner Motionpak) which forms the mounting base of the sonic anemometer. Lower-frequency motions are obtained from GPS, a gyrocompass, and the ship's Doppler speed log. Details of the motion correction are given in Edson et al. (1998) and discussion on higher-frequency data and other covariance processing issues appear in EF. Sonic temperature is corrected for velocity cross talk and the humidity contribution as in Fairall et al. (1997). The ID flux estimates are computed from the variance spectral density of u', T', and Q' in the inertial subrange of locally isotropic turbulence, which is usually at frequencies sufficiently above the wave-induced platform motions so corrections are not needed.

The optics of the high-speed hygrometer can be contaminated by salt (Fairall and Young 1991; Fairall et al. 1997) and require daily washing using specially installed water jets. Data obtained with water on the optics (e.g., during rainfall) are unreliable. In some conditions, sunlight also invalidates the data. The condition of the optics is monitored in the data stream and a threshold is set to reject such data. Because of these three sources of error, usable data for latent heat flux are significantly less than for stress. The hygrometer is located as near to the anemometer as flow distortion considerations allow (usually about 1 m), and below rather than alongside or above the anemometer. To account for the loss of correlation caused by the physical separation of the w' and Q' sensors, a correction (typically 2%–4%) is applied to $\overline{w'Q'}$ following Oncley et al. (1997).

Mean wind speed and mean vector wind magnitude are obtained from the sonic anemometer after transformation to fixed-earth coordinates. A floating thermistor is used to obtain a near-surface value for the ocean temperature (the depth is about 5 cm). The COARE cool skin algorithm is used to obtain the interface value, typically 0.3°C cooler than the bulk. Mean air temperature and humidity are obtained with a combined temperature–relative humidity sensor in an aspirated radiation shield. In the early 1990s a Vaisala HMP35 sensor (0.1°C, 3% RH quoted accuracy) was used, later replaced with a Vaisala HMP-235 (0.1°C, 2% RH quoted accuracy).

b. Flux processing methods

Covariance and ID fluxes and mean variables are computed in 10-min chunks from a nominally 1-h time section and then averaged to 1-h. A coordinate rotation of the high-speed time series is performed on the mean fixed-earth velocity vector, following Tanner and Thurtell (1969) to produce streamwise coordinates for the 1-h period. Thus, we compute fluxes normal to the mean flow vector, which is subject to a mean tilt of about 5° due to distortion by the ship's structure. Initially the 10-min covariance blocks were averaged and the ID fluxes were computed from the 1-h-averaged spectra. After 1993 we changed to spectral processing for the covariances, too. The time series is time tapered with a Hamming window, the cospectra computed, and the covariances obtained as the integral of the windowed cospec-

trum. This reduces the sampling noise caused by leakage of low-frequency variations associated with the rectangular window.

Inertial-dissipation flux techniques are based on the similarity in inertial subrange of locally isotropic turbulence that is normally observed at size scales between the production of turbulent kinetic energy (large scales) and the dissipation of energy (small scales). The wavenumber spectral density in the inertial subrange can be represented as

$$s_x(k) = 0.25C_x^2k^{-5/3} = \gamma_x N_x \varepsilon^{1/3}. \quad \text{(A1)}$$

Here k is the wavenumber, C_x^2 is the structure function parameter, γ_x is the Kolmogorov constant, N_x is the rate of dissipation for the variable x, and ε is the rate of dissipation of TKE. In the first relationship the factor 0.25 is a mathematical constant that follows from the Fourier transform relationship between the variance spectrum and the autocorrelation coefficient while, in the second, the Kolmogorov constants are empirically determined by measurements. The structure function parameter specifies small-scale turbulent fluctuations as the mean square difference in the variable x at locations separated by a small distance d:

$$C_x^2 = \overline{[x(r) - x(r + d)]^2}/d^{2/3}. \quad \text{(A2)}$$

This notation is standard in spectral analysis, and should not be confused with the transfer coefficient as used in (2) and subsequently in the body of this paper.

The ID fluxes are computed from structure function parameter relationships as described by Fairall and Larsen (1986), Edson et al. (1991), Fairall et al. (1997), and EF. Frequency spectra are computed from the time series and structure functions from the variance spectra as

$$C_x^2 = 4U_r^{-2/3}\omega^{5/3}s_x(\omega)f_{\text{tay}}, \quad \text{(A3)}$$

where U_r is the wind speed relative to the ship, ω is the angular frequency, and f_{tay} is a correction for deviations from Taylor's hypothesis associated with wind variations. To verify the $k^{-5/3}$ dependence, the spectral slope is computed as a function of frequency from a number of values in the inertial subrange (usually about 1–2 Hz) and a median C_x^2 is obtained.

MOST structure-function-relationships of the form

$$C_x^2 = x_*^2 z^{-2/3} F_x(\zeta), \quad \text{(A4)}$$

(where F_x are the MOST dimensionless function parameters) are used to compute the MOST scaling parameters

$$x_* = \pm\left[\frac{z^{2/3}C_x^2}{F_x(\zeta)}\right]^{1/2}. \quad \text{(A5)}$$

The square root creates a sign ambiguity that we resolve by giving T_* and q_* the same sign as their air–sea mean differences. We have used the F_x forms from EF; we use bulk estimates of ζ in (A5) to avoid convergence problems in the ID algorithm.

The relationship between structure functions and dissipation rates (A1) offers an alternative approach to deducing the fluxes. Using (A1) and (A3) the measured structure functions can be converted to dissipation rates, which also obey MOST. For example,

$$\varepsilon = \frac{u_*^3}{\kappa z}\phi_\varepsilon(\zeta) \quad \text{(A6a)}$$

$$N_x = \frac{u_* x_*^2}{\kappa z}\phi_{Nx}(\zeta), \quad \text{(A6b)}$$

where ϕ_ε is the MOST dimensionless TKE dissipation rate function and ϕ_{Nx} is the scalar dimensionless dissipation rate. Thus, scaling parameters computed similar to (A5) can be used based on inferred dissipation rates. Note, the dissipation rates are *inferred* rather than measured [i.e., through the empirical relationship (A1)]. Direct measurement of dissipation rates requires integration of the derivative spectrum into the kHz range, which is not feasible over the ocean. Equivalently, (A1) can be used to determine relationships between the dimensionless dissipation functions and the dimensionless structure functions:

$$F_x(\zeta) = 4.0\gamma_x\kappa^{-2/3}\phi_{Nx}(\zeta)\phi_\varepsilon(\zeta)^{-1/3}. \quad \text{(A7)}$$

Practitioners of the TKE–ID [i.e., (A6)] approach use arguments about the empirically determined balance of the TKE and variance budget equations (e.g., Taylor and Yelland 2000). For example, measurements have shown that the transport terms approximately cancel so dissipation is balanced by gradient and buoyant production:

$$\phi_\varepsilon(\zeta) = \phi_m(\zeta) - \zeta. \quad \text{(A8)}$$

The structure function–based approach that we are using employs F_x functions from EF that are fits of spectral C_x^2 values multiplied by $z^{2/3}$ and normalized by covariance values of x^2 determined on R/P *FLIP*. Here directly measured fluxes are related to directly measured structure functions through a pair of empirically determined coefficients. The TKE approach relies on determination of the terms of the TKE budget equation, the value selected for the Kolmogorov constants, and other empirical functions such as ϕ_m. The EF approach makes no assumptions about TKE balances or Kolmogorov constants; it is a simple semiempirical combination of measured inertial subrange structure function parameters, covariance fluxes, and stability.

c. Accuracy considerations

Covariance flux estimates are subject to random sampling errors associated with atmospheric variability (Wyngaard 1973; Finkelstein and Sims 2001) and other random errors caused by imperfect motion corrections or sensor noise and drift. Systematic errors are caused by incorrect sensor calibration, imperfect motion correction, and flow distortion. Of all the turbulent quantities over the ocean, the wind components (needed for

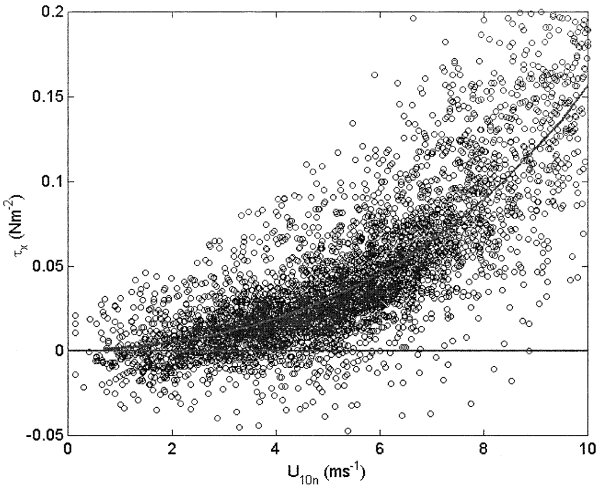

FIG. A1. Covariance measurements of the streamwise momentum flux (τ_x) as a function of 10-m neutral wind speed. The individual points are nominal 1-h averages. The solid line is COARE 3.0.

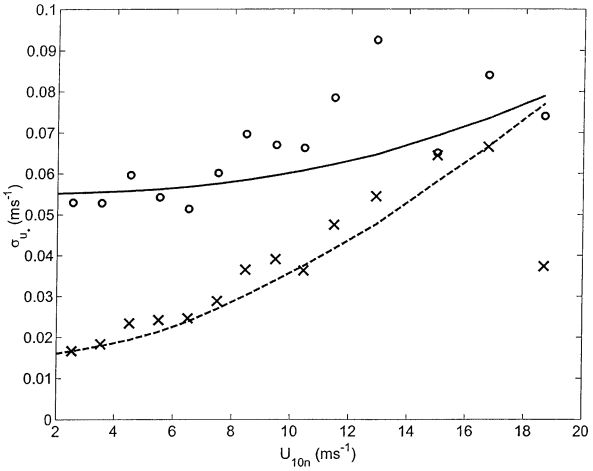

FIG. A2. Std dev of u_* within bins of mean 10-m neutral winds: ○ symbols are covariance [solid line = $(0.055^2 + 0.0036U_{10n}^2)^{1/2}$]; × symbols are ID [dashed line = $(0.015^2 + 0.0064U_{10n}^2)^{1/2}$]. Std dev is computed from the width of the distribution rather than the sum of the squares of the deviations from the mean.

the stress measurement) have the strongest signals, and the most dependable sensor. However, because of the cross talk between velocity components, stress is most susceptible to motion correction and flow distortion. Correlations between w' and sonic-derived T' are also subject to cross-talk errors because both are determined from the same time-of-flight measurements. Even humidity flux is subject to cross talk because of acceleration effects on the hygrometer's rotating light beam chopper. These effects are discussed in detail in Fairall et al. (2000) and McGillis et al. (2001). Near-zero flux measurements when ΔT and Δq are very small indicates that cross-talk errors in our scalar fluxes are small, but in the case of sensible *heat* flux they may not be negligible. The accuracy of humidity fluxes is mainly constrained by uncertainty in the response of the humidity sensor to moisture fluctuations in the flux-containing frequency range. Comparisons between sensors of similar and different types suggests this is about 5% with the sensor used here.

For well-placed sensors on ships, flow distortion is a serious concern only for stress. Stress measurements from two research vessels were found to be 10%–15% greater than those obtained on R/P *FLIP* (considered to be largely distortion and motion free) during side-by-side intercomparisons (Edson et al. 1998; EF). The distortion effect will depend on the specific arrangement of sensors relative to the ship structure, so the above results may not translate exactly to the present measurements. Therefore we have applied no empirical distortion correction to our covariance stress data but note a possible systematic uncertainty of about 10%.

The covariance stress vector is composed of streamwise (τ_x) and cross-stream (τ_y) horizontal components, which combine to give a magnitude of the stress vector, $\tau = \sqrt{\tau_x^2 + \tau_y^2}$. Figure A1 shows a scatterplot of streamwise covariance stress measurements to illustrate that negative values are part of the normal distribution of individual components. To produce bin-averaged results, such as in section 4, some researchers favor computing the magnitude of the stress vector for each 1-h estimate and then averaging. However, random errors (e.g., sampling errors) will bias such an average so we compute means for the individual components. Suppose τ_y is negligible, then τ is equal to the absolute value of τ_x. It is clear that taking the absolute value of the points in Fig. A1 and then performing an average will not yield the correct average stress on the ocean. For wind speeds above 3 m s^{-1}, τ_y makes a negligible contribution to the magnitude of the average stress. At very low winds there is a tendency for the streamwise component to average to a negative value that is interpreted as the return of momentum to the atmospheric by waves (Grachev and Fairall 2001). This effect represents another difficulty in MOST; nonzero cross-stream stress is also not accounted for by MOST. The bulk algorithm does not deal with these effects.

The ID flux estimates do not require motion corrections, and variance estimates (i.e., variance spectra) have smaller sampling variability than covariances (Wyngaard 1973). The statistical uncertainty of covariance and ID stress measurements is contrasted in Fig. A2 where variations about the bin medians are plotted as a function of wind speed. Here σ_{U*} is computed as one-half the difference in the stress values corresponding to 84% and 16% cumulative probability within each wind speed bin. One important difference between covariance and ID stress estimates is the positive-definite nature of ID algorithms for stress. In covariance measurements we obtain a distribution of stress values (including negatives) that we average to obtain a mean estimate. In

TABLE A1. Measurement uncertainty estimates from Fairall et al. (1996a).

Variable	Units	50-min rms	Bias*
U	m s^{-1}	0.3	±0.2
T, day	K	0.3	±0.2
T, night	K	0.2	±0.1
q	g kg^{-1}	0.3	±0.2
T_s	K	0.1	±0.2
q_s	g kg^{-1}	0.1	±0.2
H_s covariance	W m^{-2}	3 ± 20%	±2
H_l covariance	W m^{-2}	5 ± 20%	±4
τ, covariance	N m^{-2}	0.015 ± 30%	0.002
$\|\tau\|$, ID	N m^{-2}	15%	0.002

* Bias = Average sensor − Average correct value.

ID measurements we obtain a distribution of C_x^2, which we convert to stress values and then average. This leads to a problem in strongly convective (usually weak winds) in that values for the structure functions can be measured that are not consistent with (A2). In unstable conditions, given a value of C_T^2, there is a minimum C_u^2 that is allowed by the buoyant production term in the TKE balance. If a smaller C_u^2 is measured, the results are incompatible (if an iterative scheme is used, it will not converge). Rejecting these nonconvergent cases may bias bin-averaged results.

The ID estimates are subject to another major error source: uncertainty in the dimensionless structure function parameter. We are using F_x functions from EF that are fits of spectral C_x^2 values multiplied by $z^{2/3}$ and normalized by covariance values of x_*^2 determined on R/P *FLIP*. The TKE approach is also subject to errors in the form of the dimensionless dissipation functions and in the value selected for the Kolmogorov constants (see discussion in EF).

The absolute accuracy of transfer coefficient measurements is subject to uncertainties in the mean measurements, the fluxes, and in the case of neutral transfer coefficients (or roughness length), the MOST stability functions (see discussion in Fairall et al. 1996a). Table A1 is a reproduction of accuracies claimed by Fairall et al. (1996a). These accuracies are not derived from factory calibrations for most instruments, but from comparisons with multiple instruments and platforms such as were done in the COARE, FASTEX, and the 1999 cruises on R/V *Ronald H. Brown*. In most cruises, mean and fast humidity sensors are scaled to match a high-quality handheld ventilated psychrometer; the adjustments are typically ±2%. The near-surface water temperature sensor is checked against the ship's thermosalinograph at night when vertical gradients are expected to be low. Flow distortion corrections have been applied for mean wind speed and for the height of measurements based on wind tunnel measurements (R/V *Moana Wave*) and wind flow patterns obtained by computational fluid dynamics (R/V *Knorr* and R/V *Ronald H. Brown*). Height adjustments to mean observations and ID fluxes are made as described by Yelland et al. (1998). The corrections are typically 2%–4% and the height changes on the order of 1 m. Of the 7216 1-h observations in the database, only 390 h from the R/V *Malcolm Baldridge* have no independent distortion estimates. When possible, the wind vector is referenced to the ocean surface to remove the effects of currents. For COARE the currents at a nearby buoy were used to correct the measured earth-frame wind vectors; for the 1999 cruises the ship's Doppler speed log was used as the reference in the motion corrections.

REFERENCES

Andreas, E. L, 2001: A review of the sea spray generation function for the open ocean. Preprints, *11th Conf. on Interaction of the Sea and Atmosphere*, San Diego, CA, Amer. Meteor. Soc., 1–4.

——, J. B. Edson, E. C. Monahan, M. P. Rouault, and S. D. Smith, 1995: The spray contribution to net evaporation from the sea: A review of recent progress. *Bound.-Layer Meteor.*, **72,** 3–52.

Beljaars, A. C. M., 1995: The parameterization of surface fluxes in large-scale models under free convection. *Quart. J. Roy. Meteor. Soc.,* **121,** 255–270.

——, and A. A. M. Holtslag, 1991: Flux parameterization over land surfaces for atmospheric models. *J. Appl. Meteor.,* **30,** 327–341.

Benoit, R., 1977: On the integral of the surface layer profile-gradient functions. *J. Appl. Meteor.,* **16,** 859–860.

Blanc, T. V., 1985: Variation of bulk-derived surface flux, stability, and roughness results due to the use of different transfer coefficient schemes. *J. Phys. Oceanogr.,* **15,** 650–669.

Bourassa, M. A., D. G. Vincent, and W. L. Wood, 1999: A flux parameterization including the effects of capillary waves and sea state. *J. Atmos. Sci.,* **56,** 1123–1139.

Bradley, E. F., and R. A. Weller, 1997: Fourth workshop of the TOGA-COARE air–sea interaction (flux) working group. University Corporation for Atmospheric Research Report, UCAR, Boulder, CO, 61 pp.

——, P. A. Coppin, and J. S. Godfrey, 1991: Measurements of sensible and latent heat flux in the western tropical Pacific Ocean. *J. Geophys. Res.,* **96,** 3375–3389.

——, C. W. Fairall, J. E. Hare, and A. A. Grachev, 2000: An old and improved bulk algorithm for air–sea fluxes: COARE 2.6A. Preprints, *14th Symp. on Boundary Layer and Turbulence,* Aspen, CO, Amer. Meteor. Soc., 294–296.

Brutsaert, W., 1975: A theory for local evaporation (or heat transfer) from rough and smooth surfaces at ground level. *Water Resour. Res.,* **11,** 543–550.

——, 1982: *Evaporation into the Atmosphere.* D. Reidel, 299 pp.

Businger, J. A., J. C. Wyngaard, Y. Izumi, and E. F. Bradley, 1971: Flux profile relationships in the atmospheric surface layer. *J. Atmos. Sci.,* **28,** 181–189.

Charnock, H., 1955: Wind stress on a water surface. *Quart. J. Roy. Meteor. Soc.,* **81,** 639–640.

Chang, H.-R., and R. L. Grossman, 1999: Evaluation of bulk surface flux algorithms for light wind conditions using data from the Coupled Ocean–Atmosphere Response Experiment (COARE). *Quart. J. Roy. Meteor. Soc.,* **125,** 1551–1588.

Chertock, B., C. W. Fairall, and A. B. White, 1993: Surface-based measurements and satellite retrievals of broken cloud properties in the equatorial Pacific. *J. Geophys. Res.,* **98,** 18 489–18 500.

Clayson, C. A., C. W. Fairall, and J. A. Curry, 1996: Evaluation of turbulent fluxes at the ocean surface using surface renewal theory. *J. Geophys. Res.,* **101,** 28 503–28 513.

Csanady, G. T., 2001: *Air–Sea Interaction.* Cambridge University Press, 239 pp.

DeCosmo, J., K. B. Katsaros, S. D. Smith, R. J. Anderson, W. A. Oost, K. Bumke, and H. Chadwick, 1996: Air–sea exchange of

water vapor and sensible heat: The Humidity Exchange Over the Sea (HEXOS) results. *J. Geophys. Res.,* **101,** 12 001–12 016.
Edson, J. B., and C. W. Fairall, 1998: Similarity relationships in the marine atmospheric surface layer for terms in the TKE and scalar variance budgets. *J. Atmos. Sci.,* **55,** 2311–2328.
——, ——, P. G. Mestayer, and S. E. Larsen, 1991: A study of the inertial-dissipation method for computing air–sea fluxes. *J. Geophys. Res.,* **96,** 10 689–10 711.
——, A. A. Hinton, K. E. Prada, J. E. Hare, and C. W. Fairall, 1998: Direct covariance flux estimates from moving platforms at sea. *J. Atmos. Oceanic Technol.,* **15,** 547–562.
Fairall, C. W., and S. E. Larsen, 1986: Inertial dissipation methods and fluxes at the air ocean interface. *Bound.-Layer Meteor.,* **34,** 287–301.
——, and G. S. Young, 1991: A field evaluation of shipboard performance of an infrared hygrometer. Preprints, *Seventh Symp. on Meteorological Observations and Instrumentation,* New Orleans, LA, Amer. Meteor. Soc., 311–315.
——, E. F. Bradley, D. P. Rogers, J. B. Edson, and G. S. Young, 1996a: Bulk parameterization of air–sea fluxes in TOGA COARE. *J. Geophys. Res.,* **101,** 3747–3767.
——, ——, J. S. Godfrey, G. A. Wick, J. B. Edson, and G. S. Young, 1996b: Cool skin and warm layer effects on the sea surface temperature. *J. Geophys. Res.,* **101,** 1295–1308.
——, A. B. White, J. B. Edson, and J. E. Hare, 1997: Integrated shipboard measurements of the marine boundary layer. *J. Atmos. Oceanic Technol.,* **14,** 338–359.
——, J. E. Hare, J. B. Edson, and W. R. McGillis, 2000: Measurement and parameterization of the air–sea gas transfer. *Bound.-Layer Meteor.,* **96,** 63–105.
——, ——, A. A. Grachev, E. F. Bradley, and J. B. Edson, 2001: Preliminary results from the ETL open ocean air–sea flux database. Preprints, *11th Conf. on Interaction of the Sea and Air,* San Diego, CA, Amer. Meteor. Soc., 5–8.
Finkelstein, P. L., and P. F. Sims, 2001: Sampling error in eddy correlation flux measurements. *J. Geophys. Res.,* **106,** 3503–3509.
Garratt, J. R., 1992: *The Atmospheric Boundary Layer.* Cambridge University Press, 316 pp.
Geernaert, G. L., 1987: On the importance of the drag coefficient in air–sea interactions. *Dyn. Atmos. Oceans,* **11,** 19–38.
Godfrey, J. S., and A. C. M. Beljaars, 1991: On the turbulent fluxes of buoyancy, heat, and moisture at the air–sea interface at low wind speeds. *J. Geophys. Res.,* **96,** 22 043–22 048.
Grachev, A. A., and C. W. Fairall, 1997: Dependence of the Monin–Obukhov stability parameter on the bulk Richardson number over the ocean. *J. Appl. Meteor.,* **36,** 406–414.
——, and ——, 2001: Upward momentum transfer in the marine boundary layer. *J. Phys. Oceanogr.,* **31,** 1698–1711.
Grachev, A. A., C. W. Fairall, and E. F. Bradley, 2000: Convective profile constants revisited. *Bound.-Layer Meteor.,* **94,** 495–515.
Gulev, S. K., D. Cotton, and A. Sterl, 1998: Intercomparison of the North Atlantic wave climatology from voluntary observing ships, satellite data, and modelling. *Phys. Chem. Earth,* **23,** 587–592.
Hare, J. E., P. O. G. Persson, C. W. Fairall, and J. B. Edson, 1999: Behavior of Charnock's relationship for high wind conditions. Preprints, *13th Symp. on Boundary Layers and Turbulence,* Dallas, TX, Amer. Meteor. Soc., 252–255.
Holtslag, A. A. M., E. I. F. de Bruijn, and H.-L. Pan, 1990: A high-resolution air mass transformation model for short-range weather forecasting. *Mon. Wea. Rev.,* **118,** 1561–1575.
Jabouille, P., J. L. Redelsperger, and J. P. Lafore, 1996: Modification of surface fluxes by atmospheric convection in the TOGA COARE region. *Mon. Wea. Rev.,* **124,** 816–837.
Janssen, P. A. E. M., 1999: On the effect of ocean waves on the kinetic energy balance and consequences for the inertial dissipation technique. *J. Phys. Oceanogr.,* **29,** 530–534.
Kader, B. A., and A. M. Yaglom, 1990: Mean fields and fluctuation moments in unstably stratified turbulent boundary layers. *J. Fluid Mech.,* **212,** 637–662.
Kraus, E. B., and J. A. Businger, 1994: *Atmosphere–Ocean Interaction.* Oxford University Press, 352 pp.
Liu, W. T., and J. A. Businger, 1975: Temperature profile in the molecular sublayer near the interface of a fluid in turbulent motion. *Geophys. Res. Lett.,* **2,** 403–404.
——, K. B. Katsaros, and J. A. Businger, 1979: Bulk parameterization of the air–sea exchange of heat and water vapor including the molecular constraints at the interface. *J. Atmos. Sci.,* **36,** 2052–2062.
McGillis, W. R., J. B. Edson, J. E. Hare, and C. W. Fairall, 2001: Direct covariance air–sea CO_2 fluxes. *J. Geophys. Res.,* **106,** 16 729–16 745.
Oncley, S. P., L. K. Kristensen, J. Mann, and J. C. Wyngaard, 1997: How close is close enough when measuring scalar fluxes with displaced sensors? *J. Atmos. Oceanic Technol.,* **14,** 814–821.
Oost, W. A., G. J. Komen, C. M. J. Jacobs, and C. van Oort, 2002: New evidence for a relation between wind stress and wave age from measurements during ASGAMAGE. *Bound.-Layer Meteor.,* **103,** 409–438.
Pattison, M. J., and S. E. Belcher, 1999: Production rates of sea-spray droplets. *J. Geophys. Res.,* **104,** 18 397–18 407.
Persson, O. G. P., C. W. Fairall, E. L Andreas, P. S. Guest, and D. K. Perovich, 2002: Measurements near the Atmospheric Surface Flux Group tower at SHEBA: Near-surface conditions and surface energy budget. *J. Geophys. Res.,* **107** (C10), 8045, doi: 10.1029/2000JC000705.
Redelsperger, J. L., F. Guichard, and S. Mondon, 2000: Parameterization of mesoscale enhancement of surface fluxes for regional and large-scale models. *J. Climate,* **13,** 402–421.
Smith, S. D., 1980: Wind stress and heat flux over the ocean in gale force winds. *J. Phys. Oceanogr.,* **10,** 709–726.
——, 1988: Coefficients for sea surface wind stress, heat flux, and wind profiles as a function of wind speed and temperature. *J. Geophys. Res.,* **93,** 15 467–15 472.
——, 1989: Water vapor flux at the sea surface. *Bound.-Layer Meteor.,* **47,** 277–293.
——, C. W. Fairall, G. L. Geernaert, and L. Hasse, 1996: Air–sea fluxes: 25 years of progress. *Bound.-Layer Meteor.,* **78,** 247–290.
Tanner, C. B., and G. W. Thurtell, 1969: Anemoclinometer measurements of Reynolds stress and heat transport in then atmospheric surface layer. University of Wisconsin Tech. Rep. ECOM-66-G22-F, 82 pp. [Available from U.S. Army Electronic Command, Atmospheric Sciences Laboratory, Ft. Huachuca, AZ 85613.]
Taylor, P. K., and M. A. Yelland, 2000: On the apparent ''imbalance'' term in the turbulent kinetic energy budget. *J. Atmos. Oceanic Technol.,* **17,** 82–89.
——, and ——, 2001: The dependence of sea surface roughness on the height and steepness of the waves. *J. Phys. Oceanogr.,* **31,** 572–590.
Vickers, D., and S. K. Esbensen, 1998: Subgrid surface fluxes in fair weather conditions during TOGA COARE: Observation estimates and parameterization. *Mon. Wea. Rev.,* **126,** 620–633.
Webb, E. K., G. I. Pearman, and R. Leuning, 1980: Correction of flux measurements for density effects due to heat and water vapour transfer. *Quart. J. Roy. Meteor. Soc.,* **106,** 85–100.
Webster, P. J., and R. Lukas, 1992: The Coupled Ocean–Atmosphere Response Experiment. *Bull. Amer. Meteor. Soc.,* **73,** 1377–1416.
——, C. A. Clayson, and J. A. Curry, 1996: Clouds, radiation and the diurnal cycle of sea surface temperature in the tropical western Pacific. *J. Climate,* **9,** 1712–1730.
White, A. B., C. W. Fairall, and J. B. Snider, 1995: Surface-based remote sensing of marine boundary layer cloud properties. *J. Atmos. Sci.,* **52,** 2827–2838.
Wick, G. A., W. J. Emery, L. H. Kantha, and P. Schlussel, 1996: The behavior of the bulk-skin sea surface temperture difference under varying wind speed and heat flux. *J. Phys. Oceanogr.,* **26,** 1969–1988.
Yelland, M., and P. K. Taylor, 1996: Wind stress measurements from the open ocean. *J. Phys. Oceanogr.,* **26,** 541–558.

——, B. I. Moat, P. K. Taylor, R. W. Pascal, J. Hutchings, and V. C. Cornell, 1998: Measurements of the open ocean drag coefficient corrected for airflow disturbance by the ship. *J. Phys. Oceanogr.*, **28,** 1511–1526.

Zeng, X., M. Zhao, and R. E. Dickinson, 1998: Comparison of bulk aerodynamic algorithms for the computation of sea surface fluxes using the TOGA COARE data. *J. Climate*, **11,** 2628–2644.

——, Q. Zhang, D. Johnson, and W.-K. Tao, 2002: Parameterization of wind gustiness for the computation of ocean surface fluxes at different spatial scales. *Mon. Wea. Rev.*, **130,** 2125–2133.

Zhang, G. J., and M. J. McPhaden, 1995: The relationship between sea surface temperature and latent heat flux in the equatorial Pacific. *J. Climate,* **8,** 589–605.

Zulauf, M., and S. K. Krueger, 1997: Parameterization of mesoscale enhancement of large-scale surface fluxes over tropical oceans. Preprints, *22nd Conf. on Hurricanes and Tropical Meteorology*, Ft. Collins, CO, Amer. Meteor. Soc., 164–165.